NASA/TM-2005-213530

Failure Models and Criteria for FRP Under In-Plane or Three-Dimensional Stress States Including Shear Non-Linearity

Silvestre T. Pinho
Imperial College, London, UK

Carlos G. Dávila
NASA Langley Research Center, Hampton, Virginia

Pedro P. Camanho
University of Porto, Porto, Portugal

Lorenzo Iannucci
Imperial College, London, UK

Paul Robinson
Imperial College, London, UK

February 2005

The NASA STI Program Office ... in Profile

Since its founding, NASA has been dedicated to the advancement of aeronautics and space science. The NASA Scientific and Technical Information (STI) Program Office plays a key part in helping NASA maintain this important role.

The NASA STI Program Office is operated by Langley Research Center, the lead center for NASA's scientific and technical information. The NASA STI Program Office provides access to the NASA STI Database, the largest collection of aeronautical and space science STI in the world. The Program Office is also NASA's institutional mechanism for disseminating the results of its research and development activities. These results are published by NASA in the NASA STI Report Series, which includes the following report types:

- TECHNICAL PUBLICATION. Reports of completed research or a major significant phase of research that present the results of NASA programs and include extensive data or theoretical analysis. Includes compilations of significant scientific and technical data and information deemed to be of continuing reference value. NASA counterpart of peer-reviewed formal professional papers, but having less stringent limitations on manuscript length and extent of graphic presentations.

- TECHNICAL MEMORANDUM. Scientific and technical findings that are preliminary or of specialized interest, e.g., quick release reports, working papers, and bibliographies that contain minimal annotation. Does not contain extensive analysis.

- CONTRACTOR REPORT. Scientific and technical findings by NASA-sponsored contractors and grantees.

- CONFERENCE PUBLICATION. Collected papers from scientific and technical conferences, symposia, seminars, or other meetings sponsored or co-sponsored by NASA.

- SPECIAL PUBLICATION. Scientific, technical, or historical information from NASA programs, projects, and missions, often concerned with subjects having substantial public interest.

- TECHNICAL TRANSLATION. English-language translations of foreign scientific and technical material pertinent to NASA's mission.

Specialized services that complement the STI Program Office's diverse offerings include creating custom thesauri, building customized databases, organizing and publishing research results ... even providing videos.

For more information about the NASA STI Program Office, see the following:

- Access the NASA STI Program Home Page at ***http://www.sti.nasa.gov***

- E-mail your question via the Internet to help@sti.nasa.gov

- Fax your question to the NASA STI Help Desk at (301) 621-0134

- Telephone the NASA STI Help Desk at (301) 621-0390

- Write to:
  NASA STI Help Desk
  NASA Center for AeroSpace Information
  7121 Standard Drive
  Hanover, MD 21076-1320

NASA/TM-2005-213530

Failure Models and Criteria for FRP Under In-Plane or Three-Dimensional Stress States Including Shear Non-Linearity

Silvestre T. Pinho
Imperial College, London, UK

Carlos G. Dávila
NASA Langley Research Center, Hampton, Virginia

Pedro P. Camanho
University of Porto, Porto, Portugal

Lorenzo Iannucci
Imperial College, London, UK

Paul Robinson
Imperial College, London, UK

National Aeronautics and
Space Administration

NASA Langley Research Center
Hampton, VA 23681

February 2005

Available from:

NASA Center for AeroSpace Information
7121 Standard Drive
Hanover, MD 21076-1320
301-621-0390

National Technical Information Service
5285 Port Royal Road
Springfield, VA 22161
703-605-6000

Failure models and criteria for FRP under in-plane or three-dimensional stress states including shear non-linearity

S T Pinho [a], C G Dávila [b], P P Camanho [c], L Iannucci [a], P Robinson [a]

[a] *Department of Aeronautics, South Kensington Campus, Imperial College London, SW7 2AZ, London, U.K.*

[b] *NASA Langley Research Center, Hampton, VA, USA*

[c] *DEMEGI, Faculdade de Engenharia, Universidade do Porto, Rua Dr. Roberto Frias, 4200-465 Porto, Portugal*

Abstract

A set of three-dimensional failure criteria for laminated fiber-reinforced composites, denoted LaRC04, is proposed. The criteria are based on physical models for each failure mode and take into consideration non-linear matrix shear behaviour. The model for matrix compressive failure is based on the Mohr-Coulomb criterion and it predicts the fracture angle. Fiber kinking is triggered by an initial fiber misalignment angle and by the rotation of the fibers during compressive loading. The plane of fiber kinking is predicted by the model. LaRC04 consists of 6 expressions that can be used directly for design purposes. Several applications involving a broad range of load combinations are presented and compared to experimental data and other existing criteria. Predictions using LaRC04 correlate well with the experimental data, arguably better than most existing criteria. The good correlation seems to be attributable to the physical soundness of the underlying failure models.

1 Introduction

The greatest difficulty in the development of an accurate and computationally efficient numerical procedure to predict damage has to do with how to model

the material micro-structural changes and how to relate those changes to the material response. The results of the Word Wide Failure Exercise (WWFE) [1] indicate that—even for simple unidirectional layup and in-plane loading—current failure models and criteria fall short of providing a satisfactory description and prediction of failure. In fact, the mechanisms that lead to failure in composite materials are not fully understood yet.

If composite materials are to be used in structural applications, then the understanding of how each failure mode takes place—i.e. having a physical model for each failure mode—becomes an important point of concern. These physical models should establish *when* failure takes place, and also describe the post-failure behaviour. For instance, a physical model for matrix compression failure should predict that failure occurs when some stress state is achieved, as well as *what* orientation should the fracture plane have and how much energy should the crack formation dissipate.

The main failure modes of laminated fiber-reinforced composites are:

Delamination. Composite materials made of different plies stacked together tend to delaminate. The bending stiffness of delaminated panels can be significantly reduced, even when no visual defect is visible on the surface or the free edges. The physics of delamination is to a certain degree understood, and one of the best numerical tools to predict the propagation of delamination consists on the use of Decohesion Elements. These elements have been developed [2,3], and implemented in a commercial Finite Element (FE) code [4]; no further discussion of delamination as a failure mode is thus carried here.

Matrix compression failure. What is commonly referred to as matrix compression failure is actually shear matrix failure. Indeed, the failure occurs at an angle with the loading direction, which is evidence of the shear nature of the failure process.

Fiber compression failure. This failure mode is largely affected by the resin shear behaviour and imperfections such as the initial fiber misalignment angle and voids. Typically, kinking bands can be observed at a smaller scale, and are the result of fiber micro-buckling, matrix shear failure or fiber failure.

Matrix tensile failure. The fracture surface resulting from this failure mode is typically normal to the loading direction. Some fiber splitting at the fracture surface can usually be observed.

Fiber tensile failure. This failure mode is explosive. It releases large amounts of energy, and, in structures that cannot redistribute the load, it typically causes catastrophic failure.

In this work, the LaRC03 plane stress criteria [5] are extended to account for

general three-dimensional (3D) loading and for in-plane shear non-linearity. Matrix compressive failure is addressed with a modified 3D version of the Puck [6] matrix compression failure criterion. For the fiber failure in compression, a 3D criterion based on Argon's [7] approach considering matrix failure prompted by material imperfections is used in a framework similar to the one proposed in LaRC02 [8] and LaRC03 [5]. A failure model for matrix in tension and shear is derived from Dvorak and Laws's [9] fracture mechanics analyses of cracked plies, as in LaRC03 [5].

Section 2 presents the background on damage mode-based failure criteria. The LaRC04 failure criteria are developed and proposed for each failure mode in Section 3. Examples and validation follow in Section 4, and conclusions are presented in Section 5. A summary of the LaRC04 criteria is presented in Appendix.

In the following sections, the index 1 refers to the longitudinal (fiber) direction, the index 2 refers to the in-plane transverse direction and the index 3 refers to the through-the-thickness direction.

2 Damage mode-based failure criteria

Strength-based failure criteria are commonly used to predict failure events in composite structures. A large number of continuum-based criteria have been derived to relate stresses and experimental measures of material strength to the onset of failure. París [10] discusses the *ad hoc* nature of the formulation of most strength-based criteria.

Hashin [11,12] and Puck [13,14] are credited for establishing the need for failure criteria that are based on failure mechanisms. In his 1973 proposal [11], Hashin used his experimental observations of failure of tensile specimens to propose two different failure criteria, one related to fiber failure and the other related to matrix failure. The criteria assume a quadratic interaction between the tractions acting on the plane of failure. In 1980 [12], he introduced fiber and matrix failure criteria that distinguish between tension and compression failure. Given the difficulty in obtaining the plane of fracture for the matrix compression mode, Hashin used a quadratic interaction between stress invariants. Such derivation was based on logical reasoning rather than micromechanics. Although the Hashin criteria were developed for unidirectional laminates, they have also been applied successfully to progressive failure analyses of laminates by using in-situ unidirectional strengths to account for the constraining interactions between the plies [15]. The two-dimensional versions of the failure criteria proposed by Hashin in 1973 and 1980 are summarized in Table 1.

Table 1
Hashin criteria for plane stress

Constituent	Tension	Compression
Matrix	$FI_M = \left(\frac{\sigma_2}{Y^T}\right)^2 + \left(\frac{\tau_{12}}{S^L}\right)^2$	$1973: \; FI_M = \left(\frac{\sigma_2}{Y^C}\right)^2 + \left(\frac{\tau_{12}}{S^L}\right)^2$
		$1980: \; FI_M = \left(\frac{\sigma_2}{2S^T}\right)^2 + \left[\left(\frac{Y^C}{2S^T}\right)^2 - 1\right]\frac{\sigma_2}{Y^C} + \left(\frac{\tau_{12}}{S^L}\right)^2$
Fiber	$FI_F = \left(\frac{\sigma_1}{X^T}\right)^2 + \left(\frac{\tau_{12}}{S^L}\right)^2$	$FI_F = -\frac{\sigma_1}{X^C}$

Numerous studies conducted over the past decade indicate that the stress interactions proposed by Hashin do not always fit the experimental results, especially in the case of matrix or fiber compression. It is well known, for instance, that moderate transverse compression ($\sigma_{22} < 0$) increases the apparent shear strength of a ply, which is not predicted by Hashin's criterion. In addition, Hashin's fiber compression criterion does not account for the effects of in-plane shear, which significantly reduces the effective compressive strength of a ply. Several researchers have proposed modifications to Hashin's criteria to improve their predictive capabilities.

More recently, the WWFE [16] was conducted to assess the real predicting capability of the current available failure criteria. Leading researchers in failure of composites were invited to participate in a round-robin in which they presented their approaches and predictions.

In the exercise, Hart-Smith [17,18] presented the original version of the maximum strain criterion, as well as a truncated form and a generalized form of the criterion. Gotsis et al. [19] used the maximum stress criterion, superposed with a modified distortion energy (quadratic polynomial) criterion. McCartney [20] applied the principles of mechanics at the microstructural level to predict damage formation. Rotem [21] used a criterion originally published in 1973 [11], but with the matrix failure criterion modified in order to account for axial stresses. Surprisingly, Sun and Tao [22] used the Hashin-Rotem criterion [11], even though Sun had proposed previously [23] a criterion for matrix cracking that is acknowledged to represent better the matrix failure [8]. Liu and Tsai [24] used the Tsai-Wu [25] failure criterion. Wolfe and Butalia [26] used a strain-energy based failure criterion, containing a sum on exponents of the longitudinal, transverse and shear strain energies. Edge [27] used a phenomenological approach based on the stress interaction within each failure mode, with some similarities to the maximum stress, the Hashin-Rotem [11] and Hashin [12] criteria. Zinoviev [28] used the simple maximum stress criterion. Puck and Schürmann [6] were perhaps the authors who achieved better agreement between their predictions and the experiments. Their criterion is phenomenological, as different failure modes are considered. Arguably, their model for matrix compression failure possesses the most sound physical basis

of the theories proposed in the exercise.

Several lessons can be learned from the WWFE. Firstly, most criteria were unable to capture some of the trends in the failure envelopes of the experimental results. Secondly, on what concerns phenomenological failure criteria, most expressions proposed to predict each failure mode are still to some extent empirical. It is somewhat difficult to choose between the criteria due to the lack of experimental data needed to validate them against each other. Despite several efforts to develop sound phenomenological criteria, non-phenomenological criteria like Tsai-Wu [25] are often better prediction tools than some phenomenological criteria [24]. Although test results are not provided in the WWFE for several stress combinations that remain open for discussion, significant progress was made. From the limited predictive capabilities of the most accurate analyses available, it is clear that further developments in failure model theories and criteria are required before any analysis approach can be used with confidence to predict the strength of a typical aerospace composite component.

3 LaRC04 criteria for matrix failure

3.1 Tensile matrix failure

3.1.1 Critical energy release rates for non-linear shear behaviour

This subsection generalizes the expression given by Laws [29] for the energy release rate for an elliptical crack in a composite with a non-linear shear behaviour. The procedure presented here uses Eshelby's [30] application of the eigenstrain problem to solve the stress field around an oval crack, in a framework similar to Laws's [29]. Since the referred procedure is considerably complex, and yet not devoid of approximations, an alternative generalization that leads to the same result is presented in the Appendix. This alternative generalization is much simpler, though cruder; it is pragmatic in the sense that no complex mathematical manipulations are required, and the result follows from the concept of critical energy release rate and intuitive approximations.

The Eigenstrain problem Consider an infinite solid that undergoes some physical process that will generate some inelastic strain. The physical process could for instance be plastic deformation or phase transformation. Probably due to the later, this inelastic strain is commonly called transformation strain. The problem consists in determining the stress and strain fields due to the transformation strains.

The total strain tensor ε in the transformed region is the sum of an elastic strain tensor ε^{el} with the transformation strain tensor ε^t:

$$\varepsilon = \varepsilon^{el} + \varepsilon^t. \tag{1}$$

The stresses result from the elastic component of the strain,

$$\sigma = \mathbf{C} : \varepsilon^{el} = \mathbf{C} : \left(\varepsilon - \varepsilon^t\right). \tag{2}$$

Neglecting body forces acting on the body, the equilibrium equation is

$$\nabla \cdot \sigma = \mathbf{C} : \left(\nabla \cdot \varepsilon - \nabla \cdot \varepsilon^t\right) = \mathbf{0} \tag{3}$$

and can be written as

$$\mathbf{C} : \nabla \cdot \varepsilon - \mathbf{b}^t = \mathbf{0} \tag{4}$$

where $\mathbf{b}^t$ is a fictitious body force distribution defined as

$$\mathbf{b}^t = \mathbf{C} : \left(\nabla \cdot \varepsilon^t\right). \tag{5}$$

If the transformation strains are known, then Eq. (4) can be solved for ε using Fourier transforms or Papkovich-Neuber potentials [31,32].

Consider the particular case of an elliptic region in an infinite body, undergoing change of form that, without the constraint imposed by the surrounding material would result in an arbitrary homogeneous strain ε^t. The elliptic region, defined by

$$\left(\frac{x}{a}\right)^2 + \left(\frac{y}{b}\right)^2 + \left(\frac{z}{c}\right)^2 \leq 1, \tag{6}$$

has volume V and is bounded by the surface S. The fictitious body forces are in this case nil everywhere except on the surface S where they are

$$\mathbf{b}^t = \mathbf{C} : \varepsilon^t \delta\left(\left(\frac{x}{a}\right)^2 + \left(\frac{y}{b}\right)^2 + \left(\frac{z}{c}\right)^2 - 1\right) \cdot \mathbf{n} \tag{7}$$

$\mathbf{n}$ being the normal to the ellipsoid and $\delta(\cdot)$ the Dirac delta function.

Within the ellipsoid, the total strain field $\varepsilon = \varepsilon^{el} + \varepsilon^t$ is uniform and can be expressed as [29]

$$\varepsilon = \mathbf{P} : \mathbf{C} : \varepsilon^t \tag{8}$$

where the fourth order tensor $\mathbf{P}$ results from solving Eq. (4) with $\mathbf{b}^t$ from Eq. (7), and depends on the elastic properties of the material and geometry of the ellipsoid only. The derivation of the tensor $\mathbf{P}$ can be found in Refs. [31,32]. The stress field is then obtained as

$$\sigma = \mathbf{C} : \varepsilon^{el} = \mathbf{C} : \left(\varepsilon - \varepsilon^t\right) = -\left(\mathbf{C} - \mathbf{C} : \mathbf{P} : \mathbf{C}\right) : \varepsilon^t = -\mathbf{Q} : \varepsilon^t \tag{9}$$

with

$$\mathbf{Q} = \mathbf{C} - \mathbf{C} : \mathbf{P} : \mathbf{C}. \tag{10}$$

Eshelby's inclusion problem Eshelby [30] showed that the eigenstrain problem can be used for the determination of the stress and strain fields due to an elliptic inclusion. Consider an elliptical inclusion with constitutive tensor $\mathbf{C}^*$ in a homogeneous infinite solid with constitutive tensor $\mathbf{C}$. Suppose next that the solid is loaded by a uniform stress or strain at infinity, σ^∞ and ε^∞, respectively. The stress and strain in the solid can be expressed as

$$\sigma = \sigma^\infty + \tilde{\sigma} \qquad \text{and} \qquad \varepsilon = \varepsilon^\infty + \tilde{\varepsilon} \tag{11}$$

where σ^∞ and ε^∞ are the uniform stress and strain tensors induced in the solid if the inclusion was not present, while $\tilde{\sigma}$ and $\tilde{\varepsilon}$ represent a perturbation due to the presence of the inclusion.

The perturbation due to the inclusion can be computed using the eigenstrain analogy. In fact, the stress field $\sigma = \sigma^\infty$ solves the equilibrium equations everywhere in the solid, except in the inclusion, where the error in the stress is uniform: $(\mathbf{C}^* - \mathbf{C}) : \varepsilon^\infty$. This suggests that the stress state can be corrected by using a transformation strain inside the inclusion. For the inclusion and the transformed region to be equivalent, the stress in both cases must be the same. For the case of the hypothetical transformed region, the stress is

$$\sigma = \mathbf{C} : \varepsilon^{el} = \mathbf{C} : \left(\varepsilon - \varepsilon^t\right) \tag{12}$$

while in the case of the inclusion, the stress tensor is obtained as

$$\sigma = \mathbf{C}^* : \varepsilon. \tag{13}$$

For the transformed region to be equivalent to the inclusion, then Eqs. (12) and (13) can be equated, resulting in

$$\mathbf{C} : \left(\varepsilon - \varepsilon^t\right) = \mathbf{C}^* : \varepsilon. \tag{14}$$

Decomposing the strain in its two components ε^∞ and $\tilde{\varepsilon}$, and considering Eq. (8), then Eq. (14) is obtained as

$$(\mathbf{C}^* - \mathbf{C}) : \varepsilon^\infty = [\mathbf{C} - (\mathbf{C} - \mathbf{C}^*) : \mathbf{P} : \mathbf{C}] : \varepsilon^t. \tag{15}$$

For a void, $\mathbf{C}^* = 0$ and Eq. (15) reduces to

$$\varepsilon^t = \mathbf{Q}^{-1} : \sigma^\infty. \tag{16}$$

The determination of ε^t in Eq. (16) is an important result, since the strain and stress at the cavity wall follow as

$$\varepsilon = \varepsilon^\infty + \tilde{\varepsilon} = \varepsilon^\infty + \mathbf{P} : \mathbf{C} : \varepsilon^t = \varepsilon^\infty + \mathbf{P} : \mathbf{C} : \mathbf{Q}^{-1}\sigma^\infty \tag{17}$$

$$\sigma = \mathbf{C} : \varepsilon. \tag{18}$$

The interaction energy can be defined as the energy released by the introduction of a cavity [29]. Following from Eshelby's work for a linear material [30], the interaction energy for a solid loaded at infinity can be written as

$$E_{int} = \int_V \left[\int_0^{\varepsilon^t} \sigma^\infty : d\varepsilon^t \right] dV = V \int_0^{\varepsilon^t} \sigma^\infty : d\varepsilon^t \tag{19}$$

where V is the volume of the cavity.

The solution for a crack was obtained from the solution for an ellipsoidal cavity by Laws [29]. Laws considered first an infinite elliptic cylinder by letting $c \to \infty$, then expressed the interaction energy per unit length of the cylinder in a form similar to

$$E_{int} = \pi a^2 \epsilon \int_0^{\varepsilon^t} \sigma^\infty : d\varepsilon^t, \quad \text{with } \epsilon = \frac{b}{a} \tag{20}$$

and proceeded to a crack by making $\epsilon \to 0$. Since the tensor $\mathbf{Q}$ becomes singular when $\epsilon \to 0$, but not the product $\epsilon\mathbf{Q}^{-1}$, some care has to be taken. Eq. (20) can be transformed in

$$E_{int} = \pi a^2 \int_0^{\sigma^\infty} \sigma^\infty : \epsilon\mathbf{Q}^{-1} : d\sigma^\infty. \tag{21}$$

Making $\epsilon \to 0$ and defining $\mathbf{\Lambda} = \epsilon\mathbf{Q}^{-1}$, the interaction energy can be expressed as

$$E_{int} = \pi a^2 \int_0^{\sigma^\infty} \sigma^\infty : \mathbf{\Lambda} : d\sigma^\infty \tag{22}$$

where the non-zero components of the tensor $\mathbf{\Lambda}$ were calculated by Laws [29]. Assuming a non-linear shear behaviour, Eq. (22) can then be written as

$$\begin{aligned} E_{int} &= \frac{1}{2}\pi a^2 \left(\Lambda^o_{22}\sigma^2_{22} + \Lambda^o_{23}\tau^2_{23} + 2\int_0^{\tau_{12}} \tau_{12}\Lambda^o_{12} d\tau_{12} \right) \\ &= \frac{1}{2}\pi a^2 \left(\Lambda^o_{22}\sigma^2_{22} + \Lambda^o_{23}\tau^2_{23} + 2\int_0^{\gamma_{12}} \tau_{12} d\gamma_{12} \right) \\ &= \frac{1}{2}\pi a^2 \left[\Lambda^o_{22}\sigma^2_{22} + \Lambda^o_{23}\tau^2_{23} + \chi\left(\gamma_{12}\right) \right]. \end{aligned} \tag{23}$$

where $\chi\left(\gamma_{12}\right)$ is defined as

$$\chi\left(\gamma_{12}\right) = 2\int_0^{\gamma_{12}} \tau_{12} d\gamma_{12} \tag{24}$$

and, from Laws [29],

$$\Lambda_{22}^o = \Lambda_{23}^o = 2\left(\frac{1}{E_{22}} - \frac{\nu_{21}^2}{E_{11}}\right). \tag{25}$$

It is important to take into account some simplifications of the previously presented formulation:
(i) Laws [29] derivation of the crack tensor $\mathbf{\Lambda}$ is only approximate.
(ii) The superposition principle has been used, and it is not strictly valid for a non-linear shear behaviour. It is not clear if an expression for the interaction energy such as Eq. (23) could also be derived without using superposition.

In-plane shear contribution to the critical energy release rates The in-plane shear contribution to the critical energy release rate can be computed from Eq. (23) with $\sigma_{22} \equiv \tau_{23} = 0$. Suppose that the dimension of the crack in the longitudinal direction is a_L. Proceeding like Dvorak and Laws [9], the change in cracked area for crack propagation in the transverse direction is $\partial A = 2a_L \partial a_o$ and the critical energy release rate for the case of crack propagation in the transverse direction is obtained as

$$G_c^T = \frac{\partial a_L E_{int}}{\partial A} = \frac{1}{2}\frac{\partial E_{int}}{\partial a_o} = \frac{\pi a_o}{2}\chi\left(\gamma_{12}^u\right) \tag{26}$$

where γ_{12}^u is the engineering shear strain at failure. For crack propagation in the longitudinal direction, the change in cracked area is $\partial A = 2a_o \partial a_L$ and the critical energy release rate is defined as

$$G_c^L = \frac{\partial a_L E_{int}}{\partial A} = \frac{E_{int}}{2a_o} = \frac{\pi a_o}{4}\chi\left(\gamma_{12}^u\right). \tag{27}$$

3.1.2 In-situ effect

A failure criterion to predict matrix cracking under the presence of both in-plane shear and transverse tensile stresses should represent the 'in-situ' effect occurring in laminated composites. The in-situ effect, originally detected in Parvizi's tensile tests of cross-ply glass fiber reinforced plastics [33], is characterized by higher transverse tensile and shear strengths of a ply when it is constrained by plies with different fiber orientations in a laminate, when compared with the strength of the same ply in a unidirectional laminate. The in-situ strength also depends on the number of plies clustered together, and on the fiber orientation of the constraining plies.

The orientation of the constraining plies and the number of plies clustered together also affect the crack density and the stiffness reduction of the cracked

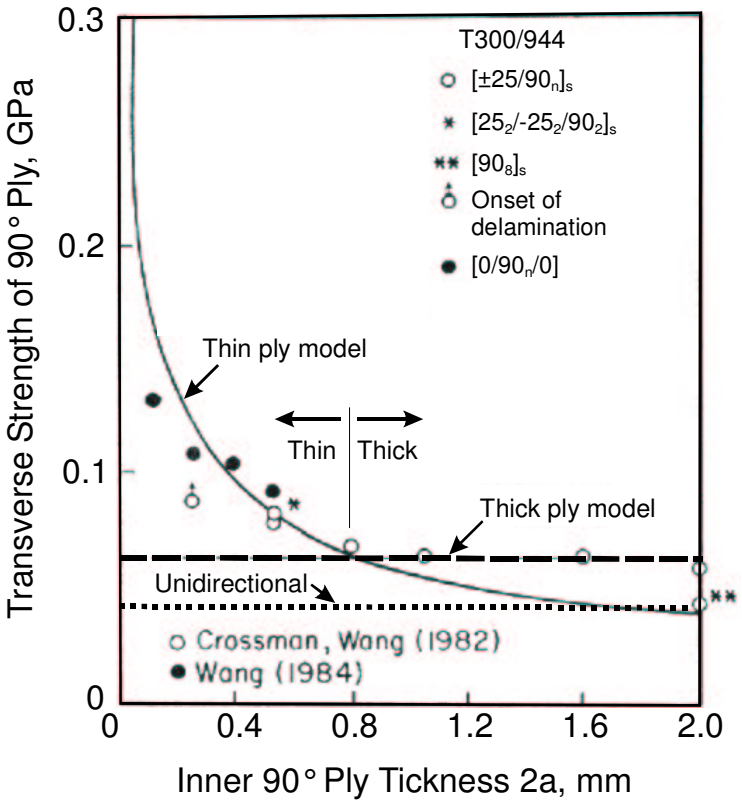

Fig. 1. Transverse tensile strength as a function of number of plies clustered together, with models from Dvorak [9] based on experimental data from Wang [34].

ply. Wang's [34] tests of $(0/90_n/0)$ $(n = 1, 2, 3, 4)$ carbon/epoxy laminates have shown higher crack densities for thinner 90° layers. The reduction of the elastic properties of a cracked ply is normally predicted using elastic analyses of cracked plies [15,35] or Continuum Damage Models [36–39].

The in-situ effect is illustrated in Fig. 1, where the relation between the in-situ transverse tensile strength and the total thickness of the 90° plies clustered together is represented.

Accurate in-situ strengths are necessary for any stress-based failure criterion for matrix cracking in constrained plies. Both experimental [34,40,41] and analytical methods [9,35,42] have been proposed to determine the in-situ strengths. In the following, the in-situ strengths are calculated using fracture mechanics solutions for the propagation of cracks in a constrained ply.

3.1.3 Fracture Mechanics Analysis of a Cracked Ply

The failure criterion for predicting matrix cracking in a ply subjected to in-plane shear and transverse tension proposed here is based on the fracture mechanics analysis of a slit crack in a ply, as proposed by Dvorak and Laws

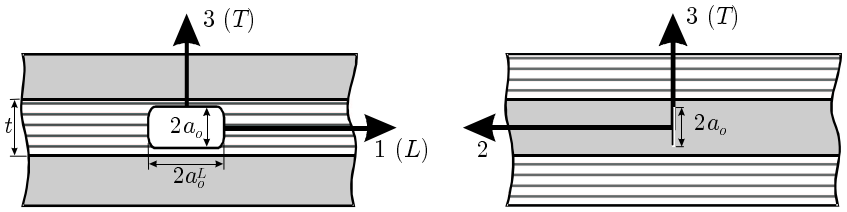

Fig. 2. Slit crack geometry (after Dvorak [9])

[9]. The slit crack represents a manufacturing defect that is idealized as lying on the $(1, 3)$ plane, as represented in Fig. 2. It has a length $2a_o$ across the thickness of a ply, t. Physically, this crack represents a distribution of matrix-fiber debonds that may be present in a ply as a consequence of manufacturing defects or from residual thermal stresses resulting from the different coefficients of thermal expansion of the fibers and of the matrix. Therefore, the slit crack is an 'effective crack,' representing the macroscopic effect of matrix-fiber debonds that occur at the micromechanical level [34].

The transverse tensile stress σ_{22} is associated with mode I loading, whereas the in-plane and transverse shear stresses τ_{12} and τ_{23} respectively are associated with mode II loading. The crack represented in Fig. 2 can grow in the 1 (longitudinal, L) direction, in the 3 (transverse, T) direction, or in both directions.

The components of the energy release rate for the crack geometry represented in Fig. 2 were determined by Dvorak and Laws [9] for a linear orthotropic material and an extension of their analysis for non-linear shear behaviour has been presented here. For mixed-mode loading, the energy release rate for crack growth in the T and L directions, $G(T)$ and $G(L)$, respectively, are given by

$$\begin{aligned} G(T) &= \tfrac{\pi a_o}{2}\left[\eta_I^2 \Lambda_{22}^o \sigma_{22}^2 + \eta_{II}^2 \Lambda_{23}^o \tau_{23}^2 + \eta_{III}^2 \chi\left(\gamma_{12}\right)\right] \\ G(L) &= \tfrac{\pi a_o}{4}\left[\xi_I^2 \Lambda_{22}^o \sigma_{22}^2 + \xi_{II}^2 \Lambda_{23}^o \tau_{23}^2 + \xi_{III}^2 \chi\left(\gamma_{12}\right)\right] \end{aligned} \tag{28}$$

where it can be observed that the energy release rate $G(L)$ for longitudinal propagation is a function of the transverse slit size and that it is not a function of the slit length in the longitudinal direction.

The parameters η_i, $i = I, II, III$ in Eq. (28) are stress intensity reduction coefficients for propagation in the transverse direction, and the parameters ξ_i, $i = I, II, III$ are reduction coefficients for propagation in the longitudinal direction. These coefficients account for the constraining effects of the adjoining layers on crack propagation: the coefficients are nearly equal to 1.0 when $2a_o \ll t$, and are less than 1.0 when $a_o \approx t$. Experimental results [41] have shown an increase in the in-situ transverse tensile strength of $[\pm\theta/90_n]_s, \theta = 0°, 30°, 60°$, laminates for increasing stiffness of adjoining sublaminates $\pm\theta$. This implies that the value of the parameter η_i decreases

with increasing stiffness of adjoining sublaminates. Considering that a transverse crack can promote delamination between the plies, Dvorak and Laws [9] suggested that the effective value of η_i can be larger than obtained from the analysis of cracks terminating at the interface, and suggested the use of $\eta_i = \xi_i = 1$.

The mode II and III components of the energy release rate are combined in a shear mode, G_{SH}, as

$$G_{SH} = G_{II} + G_{III}. \tag{29}$$

Such an approach was initially proposed by Li and Sen [43] and Li [44], and used in the simulation of delamination using the Virtual crack Closure Technique (VCCT) and decohesion finite elements [2]. By combining modes II and III, it is not necessary to track the relative orientation of the crack front with respect of the in-plane displacement jumps. In addition, no conclusive evidence is available showing that G_{IIc} and G_{IIIc} are different. In fact, there is no standard for measuring G_{IIIc}. Furthermore, there is no mixed-mode test method for mixed mode II and mode III loading.

The components of the energy release rate are then obtained for the T-direction using Eq. (28) with $\eta_i = 1$:

$$G_I(T) = \frac{\pi a_o}{2} \Lambda^o_{22} \sigma^2_{22} \tag{30}$$

$$G_{SH}(T) = \frac{\pi a_o}{2} \left[\Lambda^o_{23} \tau^2_{23} + \chi\left(\gamma_{12}\right) \right]. \tag{31}$$

The corresponding components of the fracture toughness are given as

$$G_{Ic}(T) = \frac{\pi a_o}{2} \Lambda^o_{22} \left(Y^T_{is} \right)^2 \tag{32}$$

$$G_{SHc}(T) = \frac{\pi a_o}{2} \chi\left(\gamma^u_{12_{is}} \right) \tag{33}$$

where Y^T_{is} is the in-situ transverse tensile strength, and $\gamma^u_{12_{is}}$ is the in-situ in-plane shear ultimate strain.

For propagation in the longitudinal direction, the mode I and mode II components of the energy release rate are

$$G_I(L) = \frac{\pi a_o}{4} \Lambda^o_{22} \sigma^2_{22} \tag{34}$$

$$G_{SH}(L) = \frac{\pi a_o}{4} \left[\Lambda^o_{23} \tau^2_{23} + \chi\left(\gamma_{12}\right) \right] \tag{35}$$

and the components of the fracture toughness are

$$G_{Ic}(L) = \frac{\pi a_o}{4} \Lambda^o_{22} \left(Y^T_{is} \right)^2 \tag{36}$$

$$G_{SHc}(L) = \frac{\pi a_o}{4}\chi\left(\gamma^u_{12\imath is}\right). \tag{37}$$

Having obtained expressions for the components of the energy release rate and fracture toughness, a failure criterion can be applied to predict the propagation of the slit crack represented in Fig. 2. Under the presence of in-plane and transverse shear, as well as transverse tension, the critical energy release rate G_c depends on the combined effect of all microscopic energy absorbing mechanisms such as the creation of new fracture surface. Relying on microscopic examinations of the fracture surface, Hahn [45] observed that the fracture surface topography strongly depends on the type of loading. With increasing proportion of the stress intensity factor K_{II}, more hackles are observed in the matrix, thereby indicating more energy absorption associated with crack extension. Hahn proposed a mixed-mode criterion written as a first-order polynomial in the stress intensity factors K_I and K_{II}. Written in terms of the mode I and mode II energy release rates, the Hahn criterion is

$$(1-g)\sqrt{\frac{G_I(i)}{G_{Ic}(i)}} + g\frac{G_I(i)}{G_{Ic}(i)} + \frac{G_{SH}(i)}{G_{SHc}(i)} = 1, \qquad i = T, L \tag{38}$$

where the material constant g is defined from Eqs. (36) and (37) as $g = G_{Ic}/G_{SHc}$ which leads to the following expression for g:

$$g = \frac{\Lambda^o_{22}\left(Y^T_{is}\right)^2}{\chi\left(\gamma^u_{12\imath is}\right)}. \tag{39}$$

A failure index for matrix tension can be expressed in terms of the ply stresses and in-situ strengths by substituting either Eqs. (30)-(33) or (34)-(37) into the criterion in Eq. (38) to get

$$\textbf{LaRC04 \#1} \qquad FI_M = (1-g)\frac{\sigma_{22}}{Y^T_{is}} + g\left(\frac{\sigma_{22}}{Y^T_{is}}\right)^2 + \frac{\Lambda^o_{23}\tau^2_{23} + \chi\left(\gamma_{12}\right)}{\chi\left(\gamma^u_{12\imath is}\right)} = 1. \tag{40}$$

The criterion presented in Eq. (40), with linear and quadratic terms in σ_{22}, a quadratic term in τ_{23} and a term on the in-plane shear internal energy, $\chi\left(\gamma_{12}\right)$, is similar to the criteria proposed by Hahn [45], Liu [24] (for transverse tension and in-plane shear), and Puck [6]. It can be observed that using $g = 1$ in Eq. (38) results in the linear version of the criterion proposed by Wu and Reuter [46] for the propagation of delamination in laminated composites

$$\frac{G_I}{G_{Ic}} + \frac{G_{II}}{G_{IIc}} = 1. \tag{41}$$

Furthermore, using $g = 1$, assuming linear in-plane shear, and neglecting τ_{23}, Eq. (40) reverts to the well-known Hashin criterion [11] for transverse

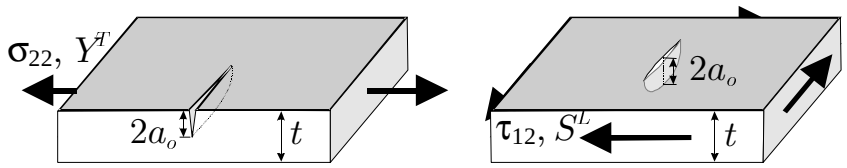

Fig. 3. Unidirectional specimen with initial crack (after Dvorak [9])

matrix cracking under both in-plane shear and transverse tension, where the ply strengths are replaced by the in-situ strengths

$$FI_M = \left(\frac{\sigma_{22}}{Y^T_{is}}\right)^2 + \left(\frac{\tau_{12}}{S^L_{is}}\right)^2 = 1. \tag{42}$$

Finally, the non-linear term in Eq. (40) is also found to be similar to the strain-energy based criterion proposed by Sandhu [47], later used by Chang and Scott [48].

3.1.4 Application to unidirectional laminates

The application of the fracture mechanics analysis of a cracked ply to unidirectional laminates yields expressions relating toughness values to crack dimensions which can subsequently be used to relate the strength of thick embedded plies to that of a unidirectional laminate.

Dvorak and Laws [9] regarded the fracture of a unidirectional specimen as the fracture of an unconstrained thick ply, with the critical initial slit crack located at the surface of the laminate. For tensile loading, the crack can be located at the edge of the laminate, which increases the energy release rate when compared with a central crack. In the case of shear loading, there is no free edge, so the crack is a central crack, as shown in Fig. 3. The defect size is $2a_o$ and is considered to be much smaller than the ply thickness, $2a_o \ll t$.

For unidirectional laminates, the crack will grow unstably in the transverse direction [9], and Eqs. (32), (33), (36) and (37) apply with a geometric factor which is obtained from the classic solution of the free edge crack [5,49], resulting in

$$G_{Ic}(T) = 1.12^2 \pi a_o \Lambda_2^o \left(Y^T\right)^2 \tag{43}$$

$$G_{SHc}(T) = \pi a_o \chi\left(\gamma^u_{12}\right) \tag{44}$$

where Y^T is the transverse tensile strength and γ^u_{12} is the in-plane shear strain at failure, for a unidirectional laminate.

The toughness ratio g can also be calculated in terms of the unidirectional

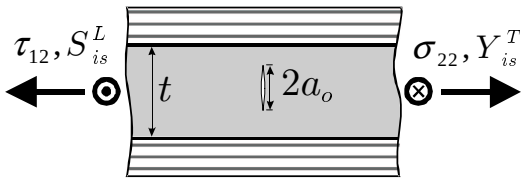

Fig. 4. Geometry of slit crack in a thick embedded ply subjected to tension and shear loads

properties by using Eq. (43) and (44), resulting in

$$g = \frac{G_{Ic}}{G_{SHc}} = 1.12^2 \frac{\Lambda^o_{22} \left(Y^T\right)^2}{\chi\left(\gamma^u_{12}\right)}. \tag{45}$$

3.1.5 In-situ strength of thick embedded plies

A thick ply is defined as one in which the length of the slit crack is much smaller than the ply thickness, $2a_o \ll t$, as illustrated in Fig. 4. The minimum thickness for a thick ply depends on the material used. For E-glass/epoxy and carbon/epoxy laminates, Dvorak and Laws [9] calculated the transition thickness between a thin and a thick ply to be approximately 0.7mm , or about 5 to 6 plies.

For the geometry represented in Fig. 4, the crack can grow in the transverse or in the longitudinal direction. Comparing Eqs. (30) and (31) to Eqs. (34) and (35), however, indicates that the energy release rate for the crack slit is twice as large in the transverse direction as it is in the longitudinal direction. Since Eqs. (30) and (31) also indicate that the energy release rate is proportional to the crack length, the crack will grow unstably in the transverse direction. Once the crack reaches the constraining plies, it can propagate in the longitudinal direction, as well as induce a delamination.

Crack propagation is predicted using Eq. (40), and the in-situ strengths can be calculated from the corresponding fracture toughness, as expressed in Eqs. (32) and (33). For mode I, the in-situ transverse tensile strength is defined from Eq. (32) as

$$Y^T_{is} = \sqrt{\frac{2G_{Ic}(T)}{\pi a_o \Lambda^o_{22}}} \tag{46}$$

and, taking into account Eq. (43),

$$Y^T_{is} = 1.12\sqrt{2} Y^T. \tag{47}$$

For a thick embedded ply loaded in pure in-plane shear, the expressions get more complex due to shear non-linearity. The in-situ in-plane ultimate strain

is obtained as

$$\gamma^u_{12|is} = \chi^{-1}\left(\frac{2G_{SHc}(T)}{\pi a_o}\right) \tag{48}$$

and, taking into account Eq. (44),

$$\gamma^u_{12|is} = \chi^{-1}\left[2\chi\left(\gamma^u_{12}\right)\right]. \tag{49}$$

Considering the constitutive law for the shear behavior to be expressed by the function f_{CL} such that

$$\tau = f_{CL}\left(\gamma\right), \tag{50}$$

then the in-situ in-plane shear strength is defined as

$$S^L_{is} = f_{CL}\left(\gamma^u_{12|is}\right). \tag{51}$$

As a particular case of non-linear in-plane shear behaviour, consider the polynomial relation between the shear strain and the shear stress proposed by Hahn and Tsai [50],

$$\gamma_{12} = \frac{1}{G_{12}}\sigma_{12} + \beta\sigma^3_{12}. \tag{52}$$

With the non-linear shear law expressed in Eq. (52), Eq. (48) reverts to

$$G_{SHc}(T) = \pi a_o\left[\frac{\left(S^L_{is}\right)^2}{2G_{12}} + \frac{3}{4}\beta\left(S^L_{is}\right)^4\right] \tag{53}$$

and Eq. (44) can be written as

$$G_{SHc}(T) = 2\pi a_o\left[\frac{\left(S^L\right)^2}{2G_{12}} + \frac{3}{4}\beta\left(S^L\right)^4\right]. \tag{54}$$

Equating Eqs. (53) and (54), the in-situ shear strength of a thick embedded ply, S^L_{is}, can be related to the shear strength of a unidirectional laminate:

$$\frac{\left(S^L\right)^2}{G_{12}} + \frac{3}{2}\beta\left(S^L\right)^4 = \frac{\left(S^L_{is}\right)^2}{2G_{12}} + \frac{3}{4}\beta\left(S^L_{is}\right)^4. \tag{55}$$

The in-situ shear strength of an thick embedded ply, S^L_{is}, is the positive, real root of Eq. (55):

$$S^L_{is} = \sqrt{\frac{\sqrt{1+\beta\left(\frac{12(S^L)^2}{G_{12}} + 18\beta\left(S^L\right)^4\right)\left(G_{12}\right)^2} - 1}{3\beta G_{12}}}. \tag{56}$$

It can be observed from Eqs. (47) and (56) that the in-situ strengths of thick embedded plies—Y^T_{is}, and S^L_{is}—are independent of the ply thickness, as has

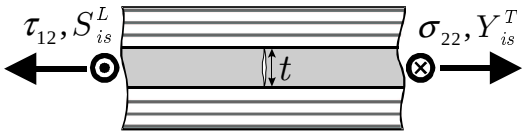

Fig. 5. Geometry of slit crack in a thin embedded ply

been observed by Dvorak and Laws [9] and Leguillon [51], and as was shown in Fig. 1. The general expression for S^L_{is} in Eq. (56) can be written for a linear material by letting β tend to zero, in which case the in-plane shear strength come as

$$S^L_{is} = \sqrt{2} S^L \qquad \text{for a linear shear law.} \tag{57}$$

Eq. (57) is equal to the one obtained by Dvorak and Laws [9] and Dávila et al. [5] for a linear shear behaviour.

3.1.6 In-situ strengths of thin embedded plies

Thin plies are defined as having a thickness smaller than the typical defect, $t < 2a_o$, so the slit crack represented in Fig. 2 extends across the entire thickness t of the ply, as represented in Fig. 5.

In the case of thin plies, crack defects can only grow in the longitudinal (L) direction, or trigger a delamination between the plies. The in-situ strengths can be calculated from the components of the fracture toughness, as expressed in Eqs. (36) and (37). For transverse tensile loading, the corresponding strength is expressed as

$$Y^T_{is} = \sqrt{\frac{8 G_{Ic}(L)}{\pi t \Lambda^o_{22}}}. \tag{58}$$

For a thin embedded ply loaded in pure in-plane shear, the ultimate in-plane shear strain is defined as

$$\gamma^u_{12 \mid is} = \chi^{-1} \left(\frac{8 G_{SHc}(L)}{\pi t} \right) \tag{59}$$

and the in-situ in-plane shear strength is defined as

$$S^L_{is} = f_{CL} \left(\gamma^u_{12 \mid is} \right). \tag{60}$$

Considering again Eq. (52) as a particular case of non-linear in-plane shear behaviour, Eq. (59) can be written as

$$\frac{\left(S^L_{is}\right)^2}{8 G_{12}} + \frac{3}{16} \beta \left(S^L_{is}\right)^4 = \frac{G_{SHc}(L)}{\pi t}. \tag{61}$$

The in-situ shear strength of a thin ply, S^L_{is}, is the positive real root of Eq.

(61):

$$S_{is}^{L} = \sqrt{\frac{\sqrt{1+\beta\frac{48G_{SHc}(L)}{\pi t}\left(G_{12}\right)^{2}}-1}{3\beta G_{12}}} \tag{62}$$

It can be observed from Eqs. (58) and (62) that the in-situ strengths are dependent on the thickness t.

Eq. (62) can be written for a linear material by letting β tend to zero, in which case the shear strength come as

$$S_{is}^{L} = \sqrt{\frac{8G_{12}G_{SHc}(L)}{\pi t}} \qquad \text{for a linear shear law.} \tag{63}$$

Eq. (63) is equal to the one obtained by Dvorak and Laws [9] and Dávila et al. [5] for a linear shear behaviour.

If in the absence of specific data, the toughness values $G_{Ic}(L)$ and $G_{SHc}(L)$ can be assumed to have the values measured by standard Fracture Mechanics tests, such as the DCB for mode I and the ENF test for mode II. Using Eq. (58), Dvorak and Laws [9] obtained a good correlation between the predicted and experimentally obtained in-situ tensile strengths of both thick and thin 90° plies in $[0/90_n/0]$ laminates, as was shown in Fig. 1.

3.2 Compressive matrix failure

Matrix compression specimens fail by shear, which would suggest that the angle of the fracture surface with the through-the-thickness direction, as shown in Fig. 6(a), should be $\alpha_o = 45^\circ$, i.e., along the plane of the maximum shear stress. However, experiments indicate that the angle of fracture under uniaxial compression is generally $\alpha_o = 53 \pm 2^\circ$ for most technical composite materials [6,52,53]. The fact that $\alpha_o > 45^\circ$ can be explained by the existence of a compressive stress acting on the potential fracture surfaces, and its associated friction. The magnitude of the compressive stress, and hence the friction stress, is maximum for a fracture surface with $\alpha_o = 0^\circ$ and decreases monotonically until $\alpha_o = 90^\circ$, in which case the compressive (and friction) stress is zero. Although the shear stress is maximum for $\alpha_o = 45^\circ$, the friction stress which opposes fracture, decreases with larger values of the angle α_o. As a result, fracture is expected for values of α_o larger than 45°, where a critical combination of shear and normal stress acts.

Experimental evidence on the fracture surface of specimens failing by matrix compression suggest that the Mohr-Coulomb (M-C) criterion is applicable to the matrix compression failure; Puck [13] and Puck and Schneider [14] were

the first to propose a matrix failure model for composites based on the M-C criterion.

The M-C criterion is commonly used in applications where fracture under tension loading is different from fracture under compression loading, such as in soil mechanics or in the fracture of cast iron. The application of the M-C criterion to multiaxial failure of epoxy resins was studied by Kawabata [54] based on correlation with his own test results. While studying the failure of chopped glass-fiber/epoxy mat laminates under confining pressures, Boehler and Raclin [55] found the Tsai-Wu criterion to be inadequate, and formulated a shearing criterion based on the M-C criterion that fit his experimental measurements well. Taliercio and Sagramoso [56] used the M-C criterion within a non-linear micromechanical model to predict the macroscopic strength properties of fiber composites.

The M-C criterion is represented geometrically by the diagram illustrated in Fig. 6(b). The Mohr's circle represents a state of uniaxial compression. The angle of the plane of fracture is α_o. The M-C criterion postulates that in a state of biaxial normal stress, fracture occurs for any Mohr's circle that is tangent to the M-C fracture line.

DiLandro and Pegoraro [57] explain the role of internal friction on the strength of carbon-fiber composites by noting the absence of chemical bonds between fiber and matrix, and that adhesion is attributed to Van der Waal's interactions. When subjected to an external load, the shear slipping of the two phases is prevented until the shear stress at the fiber-matrix interface reaches a limiting value. DiLandro and Pegoraro also note that the friction coefficient is an empirical factor that encompasses all chemical-physical interactions, including the thermal residual shrinkage of the matrix around the fiber. Larson and Miles [58] examined the relative effects of interfacial friction and roughness on the length of interfacial sliding which proceeds from the tip of an impinging fracture oriented perpendicular to the interface. According to Larson, sliding is key to the cracking behavior of fibrous brittle matrix composites in that it affects the stress concentration on the fibers, the matrix crack spacing, and, therefore, the global toughness of a composite material.

For a general loading situation, shown in Fig. 6(c), the angle of the fracture plane with the through-the-thickness direction, denoted as α, might assume a different value than the one for pure compression (α_o). The orientation of the fracture plane depends on the particular combination of shear (τ^T and τ^L) and normal (σ_n) tractions for each value of α, shown in Fig. 6(d). In plane-stress formulations, the tractions at potential fracture planes are obtained from the in-plane shear stress τ_{12}, the compressive stress σ_{22}, and the fracture plane

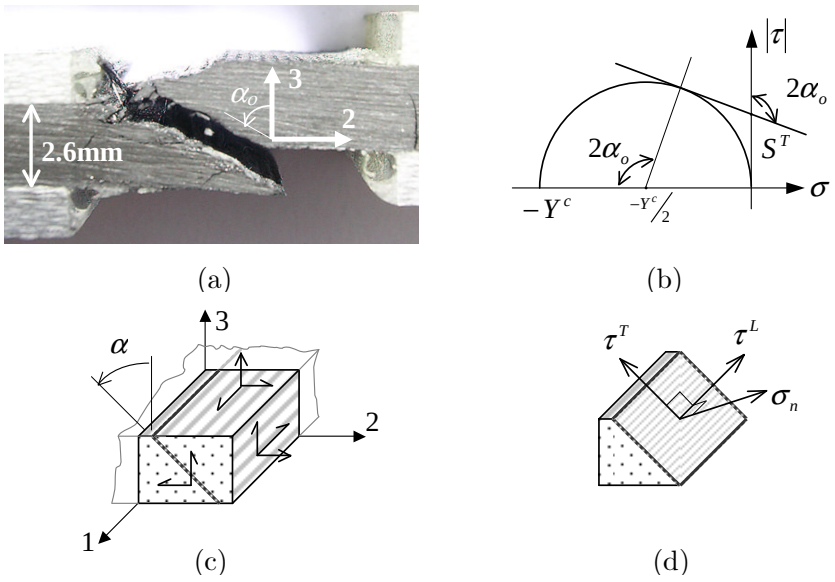

Fig. 6. (a) Pure transverse compression failure, for a CFRP specimen; (b) stresses in the fracture plane; (c) geometrical representation of the Mohr-Coulomb criterion; (d) fracture plane for a 3D stress state;

angle α by using the transformation equations

$$\begin{cases} \sigma_n = \dfrac{\sigma_{22}}{2}\left(1+\cos\left(2\alpha\right)\right) \\ \tau^T = -\dfrac{\sigma_{22}}{2}\sin\left(2\alpha\right) \\ \tau^L = \tau_{12}\cos\left(\alpha\right). \end{cases} \tag{64}$$

In a 3D formulation, the tractions are obtained from the components of the stress tensor and the fracture plane angle α:

$$\begin{cases} \sigma_n = \dfrac{\sigma_{22}+\sigma_{33}}{2} + \dfrac{\sigma_{22}-\sigma_{33}}{2}\cos\left(2\alpha\right) + \tau_{23}\sin\left(2\alpha\right) \\ \tau^T = -\dfrac{\sigma_{22}-\sigma_{33}}{2}\sin\left(2\alpha\right) + \tau_{23}\cos\left(2\alpha\right) \\ \tau^L = \tau_{12}\cos\left(\alpha\right) + \tau_{31}\sin\left(\alpha\right) \end{cases} \tag{65}$$

where α is comprised in the interval $]-\pi,\pi]$.

The M-C failure criterion is expressed in terms of the tractions in the fracture plane, and can be written in several forms. Considering first the case where $\tau^L = 0$ (i.e., $\tau_{12} = 0$ for the 2D formulation), the M-C criterion can be expressed as

$$\left|\tau^T\right| + \eta^T \sigma_n = S^T \tag{66}$$

where η^T is a friction coefficient and S^T is the transverse (to the fibers) shear strength. The geometrical representation of this criterion in a (σ,$|\tau|$) space is a line with negative slope ($-\eta^T$), shown in Fig. 6(b). In this figure, the Mohr

circle corresponding to the case of pure compression is represented through a semi-circumference tangent to the M-C criterion's line. The slope of the M-C criterion's line can be related to the angle of the fracture plane in pure transverse compression, α_o, through

$$\tan(2\alpha_o) = -\frac{1}{\eta^T}. \tag{67}$$

Furthermore, writing Eq. (66) for a pure compression case establishes the relation between S^T, Y^C and α_o:

$$S^T = Y^C \cos(\alpha_o) \left(\sin(\alpha_o) + \frac{\cos(\alpha_o)}{\tan(2\alpha_o)} \right). \tag{68}$$

The angle α_o can be easily determined from simple compression tests. The parameters η^T and S^T are calculated from α_o using Eqs. (67) and (68).

The M-C criterion (Eq. (66)) can be expressed in several forms, namely considering that friction affects (increases) the strength,

$$\frac{\left|\tau^T\right|}{S^T - \eta^T \sigma_n} = 1, \tag{69}$$

or that is affects (decreases) the applied stress,

$$\frac{\left\langle \left|\tau^T\right| + \eta^T \sigma_n \right\rangle}{S^T} = 1, \tag{70}$$

where the operator $\langle \cdot \rangle$ is the Mc Cauley bracket defined by

$$\langle x \rangle = \begin{cases} 0 \Leftarrow x \leq 0 \\ x \Leftarrow x > 0 \end{cases}, \qquad x \in \mathbb{R}. \tag{71}$$

Motivated by those two different forms of expressing the same criterion for $\tau^L = 0$, Puck and Schürmann [6,52] initially proposed for the general case ($\tau^L \neq 0$)

$$FI_M = \left(\frac{\tau^T}{S^T - \eta^T \sigma_n} \right)^2 + \left(\frac{\tau^L}{S^L - \eta^L \sigma_n} \right)^2 \leq 1 \tag{72}$$

whereas it was proposed, first for the LaRC02 [8], and after for the LaRC03 [1] [5] failure criteria

$$FI_M = \left(\frac{\left\langle \left|\tau^T\right| + \eta^T \sigma_n \right\rangle}{S^T} \right)^2 + \left(\frac{\left\langle \left|\tau^L\right| + \eta^L \sigma_n \right\rangle}{S^L} \right)^2 \leq 1 \tag{73}$$

[1] For the LaRC03 criteria [5], the in-situ longitudinal shear strength S^L_{is} was considered in equation 73 instead of S^L

where $\eta^T\sigma_n$ and $\eta^L\sigma_n$ are shear stresses due to friction. While Puck and Schürmann (Eq. (72)) consider that the compression stress (σ_n) increases the effective strength, LaRC02 and LaRC03 (Eq. (73)) consider that the compression stress reduces the effective shear stress. For reasons of simplicity, Puck and Schürmann [6,52] transformed Eq. (72) into

$$FI_M = \frac{\left(\tau^T\right)^2}{\left(S^T\right)^2 - 2\eta^T S^T \sigma_n} + \frac{\left(\tau^L\right)^2}{\left(S^L\right)^2 - 2\eta^L S^L \sigma_n} \leq 1. \tag{74}$$

Eq. (74) is obtained by expanding the denominators in Eq. (72) and neglecting the terms in $(\sigma_n)^2$. Puck and Schürmann [6] have shown that it is possible to solve Eq. (74) in a closed form for the angle of the fracture plane α in the case of a plane stress situation.

To obtain the friction coefficient η^L in the absence of experimental data, Puck and Schürmann [6] suggest the relation

$$\frac{\eta^L}{S^L} = \frac{\eta^T}{S^T} \tag{75}$$

where η^T is computed using Eq. 67 and S^T is computed using Eq. 68. This suggestion has also been considered for the LaRC02 [8] and LaRC03 criteria [5].

The comparison of the criteria expressed in Eqs. (72), (73) and (74) is shown in Fig. 7 for a E-glass/DY063 epoxy used in the WWFE, with material properties presented in Table 2. Also shown in Fig. 7 is the much simpler Sun [23] criterion

$$FI_M = \left(\frac{\sigma_{22}}{Y^C}\right)^2 + \left(\frac{\tau_{12}}{S^L - \eta^L\sigma_{22}}\right)^2 \leq 1. \tag{76}$$

The Sun criterion also represents a similar trend in the failure envelope, although it is not based on a physical mechanism of failure.

While the initial and final Puck criteria (Eqs. (72) and (74)) yield similar results, LaRC03 criterion (Eq. (73)) is less conservative. This is related to the fact that the effect of friction is over-estimated in Eq. (73). Indeed, affecting the shear tractions by a friction term as in Eq. (73) over-estimates the friction forces whenever both τ^T and τ^L are acting simultaneously [59]. As Fig. 8(a) represents, supposing a very simple case with isotropic friction ($\eta^T = \eta^L$), the friction stresses are over-estimated by a factor of $\sqrt{2}$ when using Eq. (73).

It is interesting to notice the effect that an orthotropic friction model has on

Table 2
Mechanical properties of a E-glass/DY063 epoxy used in the WWFE, from Soden et al. [60]

G_{12}	S^L	X^C	Y^C	α_o
(GPa)	(MPa)	(MPa)	(MPa)	(°)
5.83	73	800	145	53

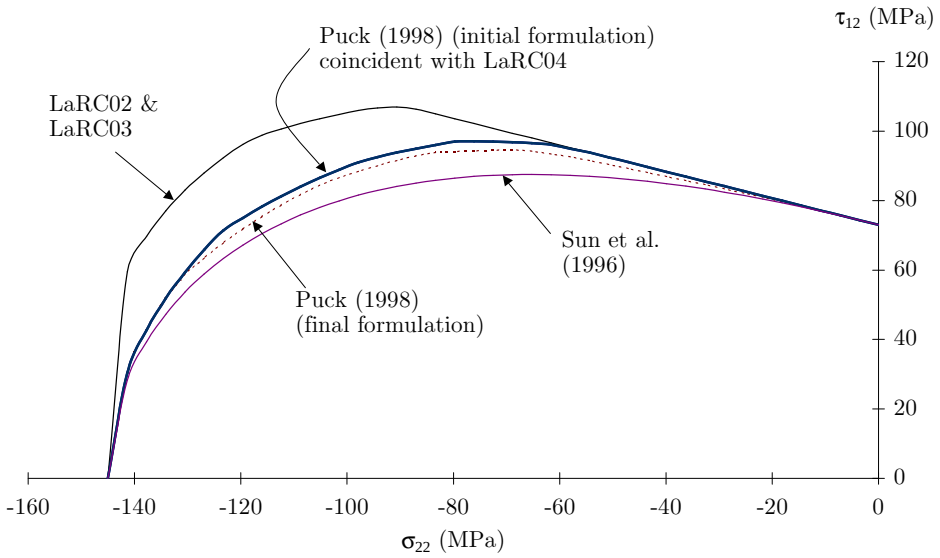

Fig. 7. Failure envelopes for transverse compression and inplane shear

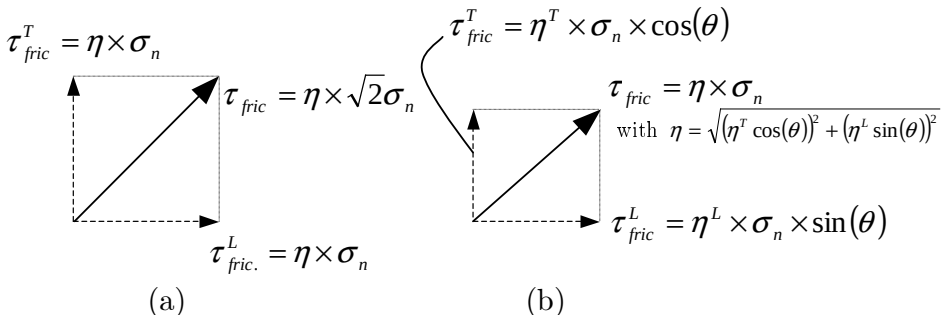

Fig. 8. (a) Overestimation of the friction stress; (b) model that does not overestimate the friction stresses

LaRC03 criterion (Eq. (73)). A reasonable model for orthotropic friction is

$$\left\{ \begin{array}{c} \tau_T^{fric.} \\ \tau_L^{fric.} \end{array} \right\} = \sigma_n \left[\begin{array}{cc} \eta^T & 0 \\ 0 & \eta^L \end{array} \right] \left\{ \begin{array}{c} \frac{\tau^T}{\|\tau\|} \\ \frac{\tau^L}{\|\tau\|} \end{array} \right\} \tag{77}$$

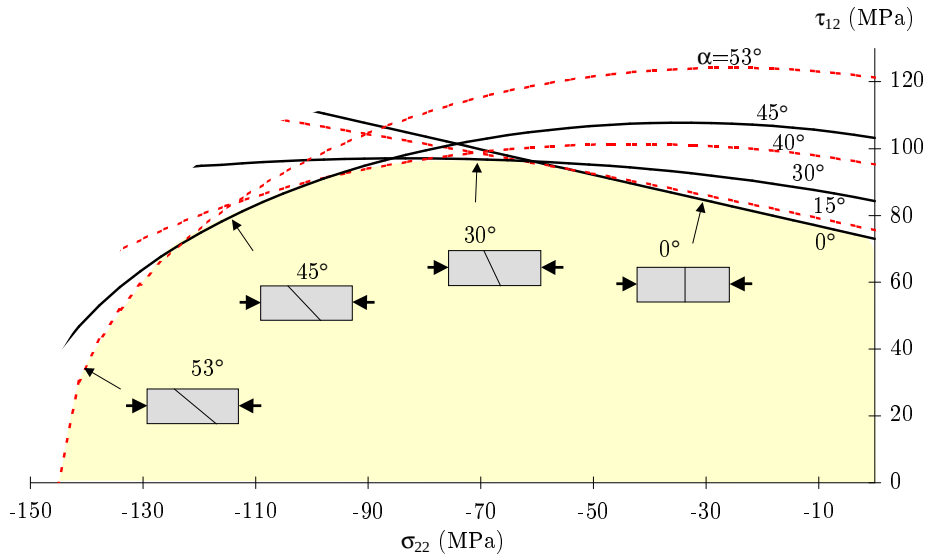

Fig. 9. Failure envelope for the LaRC04 matrix failure criterion, using Eq. 81 and several values for the angle of the fracture plane, α

or, simplifying,

$$\begin{cases} \tau_T^{fric.} = \sigma_n \eta^T \cos(\theta) \\ \tau_L^{fric.} = \sigma_n \eta^L \sin(\theta) \end{cases} \tag{78}$$

where θ is the angle formed by the shear-traction vector τ and the transverse direction in the fracture plane, i.e., $\theta = \arctan\left(\tau^L/\tau^T\right)$.

The LaRC03 criterion given by Eq. (73) can be modified using Eqs. (78) to account more accurately for the friction terms, which results in

$$FI_M = \left(\frac{\left\langle \left|\tau^T\right| + \eta^T \sigma_n \cos(\theta) \right\rangle}{S^T}\right)^2 + \left(\frac{\left\langle \left|\tau^L\right| + \eta^L \sigma_n \sin(\theta) \right\rangle}{S^L}\right)^2 \leq 1 \tag{79}$$

Interestingly, the modified criterion given by Eqs. (79) yields an envelope that is coincident with Puck's initial criterion (Eq. (72)), as shown in Fig. 7.

The use of one of Eqs. (72), (73), (74), and (79) for the failure criterion implies the use of the set of Eqs. (65) for the transformation of stresses. In turn, this means that the fracture angle has to be known. In theory, it could be analytically determined as

$$\alpha: \quad \frac{\partial FI_M}{\partial \alpha} = 0. \tag{80}$$

Puck and Schürmann [6] have solved Eq. 80 for the criterion in Eq. (74) in a plane-stress situation, but it is not possible to do the same with Eqs. (72), (73) and (79) for 3D stress states. However, Fig. 9, drawn using the data from

Table 2 and Puck's initial criterion (Eq. (72)), shows that it is possible to draw the envelope with reasonable accuracy by using a very small number of trial angles.

Since it is not possible to obtain a closed-form solution for the fracture angle in a generic 3D situation, there does not seem to be a reason to drop the physical significance of the criteria expressed through Eqs. (72), (73) and (79). As it was demonstrated, Eq. (73) over-estimates the friction stresses. Since Eqs. (72), (79) yield similar results, but Eq. (72) is simpler, the later is proposed for LaRC04,

$$\textbf{LaRC04 \#2} \qquad FI_M = \left(\frac{\tau^T}{S^T - \eta^T \sigma_n}\right)^2 + \left(\frac{\tau^L}{S^L_{is} - \eta^L \sigma_n}\right)^2 \leq 1 \quad (81)$$

where it should be noted that the in-situ longitudinal shear strength S^L_{is} is used, as was proposed for LaRC03 [5].

4 LaRC04 criteria for fiber failure

4.1 Tensile fiber failure

The LaRC04 criterion for fiber tensile failure is a non-interacting maximum allowable stress criterion. Consequently, the LaRC04 failure index for fiber tensile failure is simply

$$\textbf{LaRC04 \#3} \qquad FI_F = \frac{\sigma_{11}}{X^T} \leq 1. \quad (82)$$

4.2 Compressive fiber failure

Fiber compression failure is a field where significant research is still being performed. For matrix compression failure, a relatively simple mechanical model as the one proposed by Puck and Schürmann [6,13,14,52] seems to correctly represent failure, and can be easily expressed as a failure criterion that can be incorporated in numerical codes. Depending on the material, different fiber compressive failure modes are possible [61]:

Microbuckling. This failure mode consists of the microbuckling of the fibers in the elastic matrix. The first mechanical model for this failure mode can be tracked back to Rosen's work [62] where the fibers are represented by infinite

beams [2] in an elastic matrix and failure is attained when the compressive load equals the buckling load. This model provides an upper bound for the failure stress, as it generally predicts a failure stress typically two to three times larger than the experimental one (for carbon reinforced composites [61]). Models based on microbuckling have been widely studied over the last decades. For these models, the matrix shear properties as well as material imperfections play an important role.

Kinking. Kinking can be defined as the localized shear deformation of the matrix, along a band. Typically, the fibers break at the edges of the band, and sometimes also in the interior. It should be noted that some authors consider kinking as a consequence of microbuckling, while others consider it as a separate failure mode [61]. Argon [7] was the first to develop a mechanical model for fiber kinking as a separate failure mode. For Argon, failure is the result of matrix shear failure, prompted by an initial fiber misalignment. For this model, and those that follow it, matrix elastic behaviour and initial material imperfections play an important role.

Fiber failure. Fiber failure can be expected to occur for fibers with low compressive strength, such as Aramid, but is not expected to happen for carbon, glass or boron fibers [61].

Rosen [62] was the first to propose a mechanical model to describe fiber microbuckling. By minimizing the internal energy, Rosen obtained the fiber's buckling stresses. The analysis was performed for two instability modes: (i) an extension mode, where the deformed shapes of adjacent fibers are in opposition of phase; and (ii) a shear mode, where the deformed shapes of adjacent fibers are in phase. Rosen found that for composites with a high fiber volume fraction, the shear mode is critical, and the associated stress is

$$X^C = \frac{G_m}{1 - V_f} \tag{83}$$

where G_m is the shear modulus of the matrix and V_f is the fiber volume fraction. Considering the rule of mixtures, Eq. (83) reduces to $X^C = G_{12}$, i.e., the shear modulus of the composite. This relation (Eq. (83)) was later modified to account for an elastic-perfectly plastic resin [63]. In fact, several modifications were attempted, in order to incorporate less restrictive hypotheses (see Ref. [61] for a state of the art review). However, Rosen's approach yields smaller failure stresses than similar models assuming linear elasticity and straight fibers [61] and is simpler. Still, there is little success in predicting the failure stress of advanced composites using Rosen's result. The problem is that, when compared to experimental data, Eq. (83) gives results typically 1.5 times

[2] In fact, Rosen's approach is 2D and the fibers are thus represented by layers (plates), and not beams

higher for Boron composites, 2 to 3 times higher for carbon composites and 4 times higher for glass composites [61]. It was with the introduction of geometric non-linearity and initial fiber misalignment that the prediction got closer to the experimental results.

Schultheisz and Waas [61] pointed out that most buckling models tend to replicate the model-composite that was studied by Greszczuk [64–67]. Greszczuk performed a series of experiments on model-composites whose reinforcements consisted of either (i) rods (of steel or aluminum) having diameters in the range 0.5 to 3.2mm ; or (ii) aluminum plates with thickness in the range of 0.3 to 1mm . The basic idea was to duplicate the 2D geometries used in the analytical models. Greszczuk found that the compressive strength of his model-composites exceeded Rosen's prediction. However, when including the energy associated with bending of the fibers, Greszczuk found good agreement. He also concluded that while his model-composites with low-modulus matrix failed by microbuckling, those with intermediate-modulus matrix failed by longitudinal cracking (matrix cracking), and composites with high-modulus matrix failed through compression of the fibers.

Most buckling models follow the 2D approach of Rosen [62]. However, real technical composites are 3D structures. It has been suggested [68,69] that 3D effects may be a cause of the reduction in the failure stress from Rosen model. Indeed, evidence of the 3D aspect of fiber microbuckling has been reported in the literature [70,71]. One important 3D consideration, discussed by Schultheisz and Waas [61], is the arrangement of fibers and matrix, which induce different types of interaction (among the fibers and matrix) during the buckling for different packing densities. Furthermore, the laminated construction may lead to different fiber arrangements within the plane of a lamina and in the through-the-thickness direction. Fiber misalignment angles have first been reported to be smaller in the through-the-thickness direction [72], but more recent results suggest they are similar in magnitude [73]. Models incorporating 3D aspects were attempted [67,74–78], and Schultheisz and Waas [61] concluded that FE analysis would be an excellent candidate to handle the 3D aspect of microbuckling.

In most high fiber-volume-fraction advanced composite materials, compressive failure is seen as a failure mode which is localized in a band across the specimen in which the fibers have rotated by a large amount, and the matrix has undergone large shearing deformation—kinking. A schematic representation of a kink band is shown in Fig. 10(a). In the literature, kinking is often seen as a consequence of microbuckling, and not a failure mode itself. However, kinking is other times identified as an independent failure mode. On the discussion on whether or not kinking is a consequence of microbuckling, the main argument has to do with the orientation of the kink-band boundary. Indeed, if kinking is a consequence of microbuckling, then one would expect the kink-band bound-

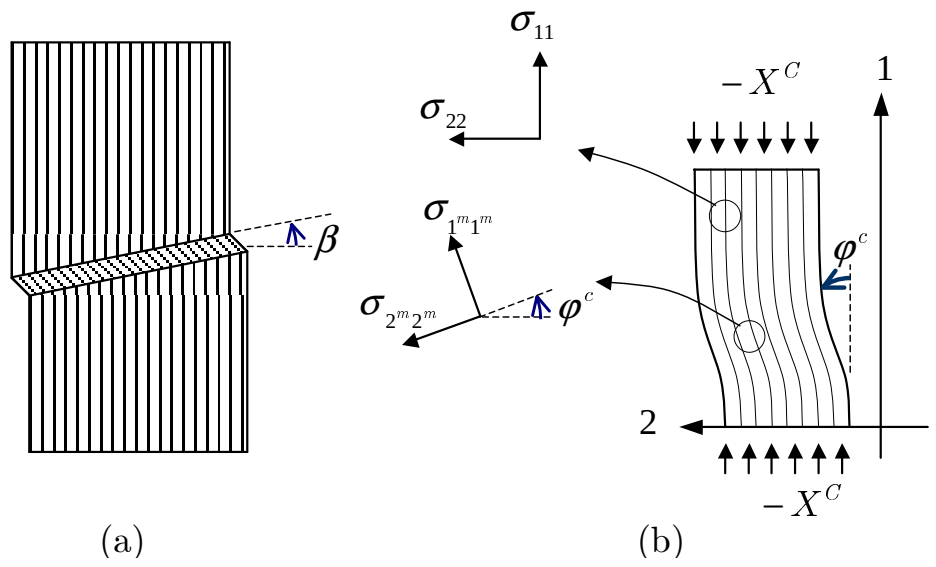

Fig. 10. (a) Kinking band; (b) fiber misalignment frame

ary to lie normal to the loading axis (original fiber direction), i.e., to lie in the plane of highest bending stresses. In Fig. 10(a), this would mean an angle β equal to zero. However, it is found that in most cases β lie in the range of 30°. On the other hand, the similarity between the kink bands and shear bands may suggest that shear is the main factor at the onset of kink-band formation. In this case, it would be expected that kink bands would occur in the planes of maximum shear stress, i.e., for $\beta = 45°$. Some thick kink bands have been found near 45° [61], but this is generally not the case.

Another argument supporting kinking as a separate failure mode was introduced by Chaplin [79], who noted that microbuckling should occur everywhere in the composite at about the same time, whereas kinking in his experiments was clearly initiated from some kind of defect.

Effendi [80] carried a set of experimental tests on different carbon-fiber composites and also carried an analytical buckling analysis, which included initial fiber waviness, and computed the stresses in the fiber and matrix constituents. He found that before the buckling load was attained, the stress levels in the constituents exceeded the respective failure stress. To refine the modelling, he conducted a numerical FE analysis, where a non-linear matrix behaviour was incorporated. The results confirmed that constituent failure happened first. Composites with small initial imperfections or weaker fiber would fail by fiber failure, while in composites with large initial imperfections or stronger fibers, the matrix would fail first.

On their review of the state of the art on compression failure of composites, Schultheisz and Waas [61] concluded that the experimental observations on the kinking phenomenon support the contention that kink bands seen in high

fiber-volume-fraction advanced composite materials occur via a mechanism that is different from the global microbuckling mode suggested by Rosen [62]. Furthermore, in advanced composites, kinking seems to be initiated by local microstructural defects, such as fiber misalignments and longitudinal (matrix or interfacial) cracking. Therefore, kinking is better understood by treating the problem of stress redistribution, including dynamics, and including both non-linear geometry and material response.

Whether kinking is a result of fiber microbuckling or a separate failure mode, it is the most common failure feature observed after testing. The kink-band angle and kink width were studied by Hahn [81] for carbon fiber composites (CFRP), glass fiber composites (GFRP) and Aramid fiber composites (AFRC). The kink-band angle β, and the band width w, were found to be the smaller for CFRP at room temperature ($\beta \approx 20^\circ$ and $w \approx 0.07$ to 0.2mm). For GFRP no clear kink bands were observed at room temperature. However, at 100°C , a kink angle $\beta \approx 30^\circ$ and a width $w \approx 1.2$mm were observed. For AFRP tested at room temperature, the kink angle was found as $\beta \approx 40^\circ$ and width $w \approx 0.45$mm . Chaplin [79] noted the angle of rotation of the fibers in the kink band was twice the angle β, so that no volumetric changes happened in the kinked region.

Argon [7] was the first researcher to provide a model for kink-band formation. In his model, it is assumed that an initial fiber misalignment exists, which leads to shearing stresses between the fibers. The shearing stresses would act as to further rotate the fibers, which would in turn lead to further increase in the shear stresses. This closed-loop effect would then lead to failure. The main result from his analysis is the relation between the compressive failure stress, X^C, the matrix in-plane shear failure stress, S^L, and the initial fiber misalignment angle φ^o:

$$X^C = \frac{S^L}{\varphi^o}. \tag{84}$$

From Argon's analysis, a kink-band angle $\beta = 45^\circ$ should also result. Several authors since reported the sensitivity of the compressive failure stress to the shear failure stress [82–85]. Budiansky [84] later extended Argon's analysis to

$$X^C = \frac{S^L}{\varphi^o + \gamma^u} \tag{85}$$

where γ^u is the shear strain at failure. Failure occurs when the shear failure stress is reached.

4.2.1 2D Kinking model

Consider a unidirectional composite with a misaligned region being compressed, as depicted in Fig. 10(b). The stresses in the misalignment frame

are

$$\begin{cases} \sigma_{1^m1^m} = \dfrac{\sigma_{11}+\sigma_{22}}{2} + \dfrac{\sigma_{11}-\sigma_{22}}{2}\cos(2\varphi) + \tau_{12}\sin(2\varphi) \\ \sigma_{2^m2^m} = \dfrac{\sigma_{11}+\sigma_{22}}{2} - \dfrac{\sigma_{11}-\sigma_{22}}{2}\cos(2\varphi) - \tau_{12}\sin(2\varphi) \\ \tau_{1^m2^m} = -\dfrac{\sigma_{11}-\sigma_{22}}{2}\sin(2\varphi) + \tau_{12}\cos(2\varphi)\,. \end{cases} \tag{86}$$

For failure under pure compression ($\sigma_{11} = -X^C$ and $\sigma_{22} \equiv \tau_{12} = 0$), Eqs. (86) lead to

$$\begin{cases} \sigma^c_{1^m1^m} = -X^C\cos^2(\varphi)\,, \\ \sigma^c_{2^m2^m} = X^C\sin^2(\varphi) \quad \text{and} \\ \tau^c_{1^m2^m} = X^C\sin(\varphi)\cos(\varphi)\,. \end{cases} \tag{87}$$

The stress state in the misalignment coordinate frame can now be used to check for fiber kinking. For a material with linear shear behaviour, replacing it in an appropriated matrix failure criterion leads directly to the expression for the specific value of the misalignment angle φ at failure for a pure compression case—φ^c. For a material with non-linear shear behaviour, it will become clear at the end of this section that kinking can result either from (i) matrix failure (i.e. the verification of a matrix failure criterion), or (ii) instability, due to the loss of (shear) stiffness for larger shear strain values.

Without loss of generality, suppose first the case of failure by the verification of an appropriate matrix failure criterion.

Case 1 *Kinking for pure compression as the result of matrix failure*

Using LaRC04 matrix compression failure criterion, Eq. (81), the expression for the specific value of the misalignment angle φ at failure for a pure compression case (φ^c) is obtained as

$$X^C\left(\sin(\varphi^c)\cos(\varphi^c) - \eta^L\sin^2(\varphi^c)\right) = S^L. \tag{88}$$

The angle φ^c is the sum of an initial misalignment with the rotation due to loading. Eq. (88) can be solved for φ^c [5], resulting in

$$\varphi^c = \arctan\left(\frac{1-\sqrt{1-4\left(\frac{S^L}{X^C}+\eta^L\right)\frac{S^L}{X^C}}}{2\left(\frac{S^L}{X^C}+\eta^L\right)}\right). \tag{89}$$

It can be observed that by neglecting η^L, and assuming φ^c to be small and constant, Eq. (88) yields Argon's equation (Eq. (84)). In fact, assuming all the above but not that φ^c is constant yields Budiansky's Eq. (85).

From the constitutive law, the shear stress in the misaligned frame is obtained

as a function of the shear strain

$$\tau_{1^m2^m} = f_{CL}(\gamma_{1^m2^m}) \tag{90}$$

and from the transformation equations (Eqs. (86)), the shear stress in the same frame for pure axial compressive failure is

$$\tau^c_{1^m2^m} = \frac{1}{2}\sin\left(2\varphi^c\right) X^C. \tag{91}$$

Equating Eqs. (90) and (91), the shear strain at failure for a pure axial compression case, $\gamma^c_{1^m2^m}$, is obtained as

$$\gamma^c_{1^m2^m} = f^{-1}_{CL}\left(\frac{1}{2}\sin\left(2\varphi^c\right) X^C\right). \tag{92}$$

For instance, for a material with a linear shear strain vs. shear stress behavior, Eq. (92) becomes simply

$$\gamma^c_{1^m2^m} = \frac{\sin\left(2\varphi^c\right) X^C}{2G_{12}}. \tag{93}$$

Assuming small angle approximations, a simpler expression for Eq. (93) can be obtained,

$$\gamma^c_{1^m2^m} = \frac{\varphi^c X^C}{G_{12}}. \tag{94}$$

Either way, the initial misalignment angle comes then as

$$\varphi^o = \varphi^c - \gamma^c_{1^m2^m} \tag{95}$$

where $\gamma^c_{1^m2^m}$ can be defined through Eqs. (92), (93) or (94).

Writing Eq. (92) in the form

$$f_{CL}\left(\gamma^c_{1^m2^m}\right) = \frac{1}{2}\sin\left[2\left(\varphi^o + \gamma^c_{1^m2^m}\right)\right] X^C \tag{96}$$

and plotting the left and right hand side of it in a (γ, τ) space and provides insight into the meaning of the solution of Eq. (92). Fig. 11(a) represents both sides of Eq. (96) for a material with linear shear behaviour.

The Left Hand Side (LHS) of Eq. (96) is the shear strain vs. shear stress material law. The Right Hand Side (RHS) of Eq. (96) represents the shear stress resulting from the compressive longitudinal loading, in a rotated coordinate system. As the compressive stress increases, the 'RHS' curve corresponding to a general stress level shifts up, and the intersection with the 'LHS' curve defines the strain in the misalignment frame $\gamma_{1^m2^m}$. At failure (when the compressive stress equals X^C), the strain in the misalignment frame is defined as $\gamma^c_{1^m2^m}$ and is shown in Fig. 11(a).

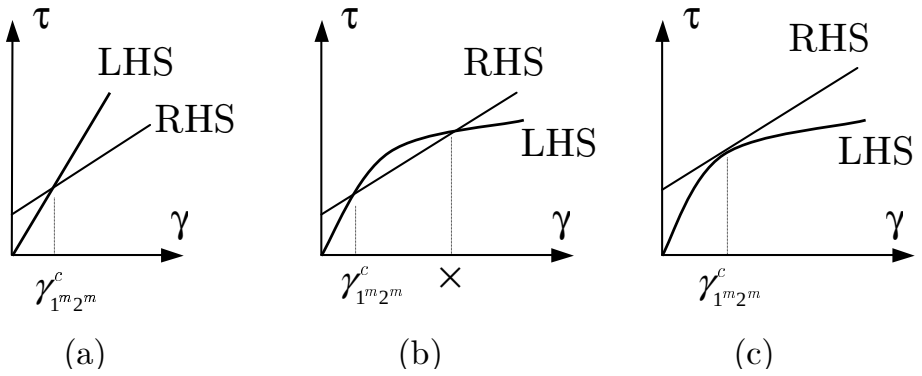

Fig. 11. Left and Right hand side of Eq. (96), for a material with a (a) linear shear behavior, (b) non-linear shear behavior, and failure by matrix cracking, and (c) non-linear shear behavior, and failure by instability

For a material with non-linear shear behaviour, there could be more than one intersection point for each stress level, as represented in Fig. 11(b) for the particular case of failure onset. For such a non-linear material, the equilibrium position, which defines the orientation of the misaligned frame, corresponds to the first intersection (lower energy). As the compressive loading increases, the 'RHS' curve corresponding to a general stress level shifts up, and the intersection with the 'LHS' curve defines the strain in the misalignment frame $\gamma_{1^m2^m}$. At failure (when the compressive stress equals X^C), the strain in the misalignment frame is defined as $\gamma^c_{1^m2^m}$ and is shown in Fig. 11(b). Therefore, $\gamma^c_{1^m2^m}$ has to correspond to the first intersection of the two curves. However, this is not guaranteed by the solution of Eqs. (89), (92) and (95). If the referred solution corresponds to the second intersection, then the solution is not valid and failure is due to a different mechanism, which is now discussed.

Case 2 *Kinking for pure compression as the result of instability*

A second mechanism that can promote fiber kinking is elastic instability of the matrix, due to the softening character of the constitutive law. As a composite is progressively loaded in compression, the curve 'RHS' in Fig. 11(b) shifts up, also progressively. Suppose that at the moment the two curves ('LHS' and 'RHS') are tangent to each other, Fig. 11(c), the matrix compression failure criterion (LaRC#2, Eq. (81)) is not yet verified. Then, a small increase in the compressive load results in the two curves not touching each other. Physically, this means that there is no equilibrium position and catastrophic failure results, due to unstable rotation of the fibers. It is concluded that the compressive strength measured for pure axial compression is in this case actually a failure due to instability, rather than matrix failure.

The values of φ^o and $\gamma^c_{1^m2^m}$ corresponding to this type of failure can be obtained from the system that results from Eq. (96) and the condition that

expresses that the left and right hand side of Eq. (96) have the same slope at $\gamma^c_{1^m2^m}$:

$$\begin{cases} f_{CL}(\gamma^c_{1^m2^m}) = \dfrac{X^C}{2}\sin\left[2\left(\varphi^o+\gamma^c_{1^m2^m}\right)\right] \\ \left.\dfrac{\partial f_{CL}(\gamma_{1^m2^m})}{\partial\gamma_{1^m2^m}}\right|_{\gamma^c_{1^m2^m}} = X^C\cos\left[2\left(\varphi^o+\gamma^c_{1^m2^m}\right)\right]. \end{cases} \tag{97}$$

To summarize, the three variables φ^o, $\gamma^c_{1^m2^m}$ and φ^c can be determined by Eqs. (89), (92) and (95) (matrix compressive failure) or by Eqs. (95) and (97) (elastic instability).

If the instability solution occurs for $F_M < 1$ (in LaRC#2, Eq. (81)), then the instability solution must be considered; otherwise the matrix compressive failure solution is considered. Either way, φ^o, $\gamma^c_{1^m2^m}$ and φ^c are always defined.

The initial misalignment angle φ^o is a material property, and could be regarded as an equivalent angle that embodies microstructural defects (that can trigger kink-band formation) other than the initial misalignment, like oscillations in the fiber volume fraction or in the bonding to the resin. Knowing φ^o allows the establishment of an equation defining the misalignment angle for a generic plane stress situation, φ, by using the transformation Eqs. (86),

$$f_{CL}(\gamma_{1^m2^m}) = -\frac{\sigma_{11}-\sigma_{22}}{2}\sin\left(2\left(\varphi^o+\gamma_{1^m2^m}\right)\right)+|\tau_{12}|\cos\left(2\left(\varphi^o+\gamma_{1^m2^m}\right)\right) \tag{98}$$

and the angle φ is obtained from

$$\varphi = \frac{\tau_{12}}{|\tau_{12}|}\left(\varphi^o+\gamma_{1^m2^m}\right). \tag{99}$$

Note that, in Eq. (98), $|\tau_{12}|$ was used instead of τ_{12} because it is the easiest way of considering simultaneously the possibility of an initial misalignment $\pm\varphi^o$.

Solving this equation (where for any load case the only unknown variable is $\gamma_{1^m2^m}$) for non-linear shear responses is probably the most complex task of the whole model. For most practical cases, Eq. (98) can be simplified without significant error by assuming small angle approximations:

$$f_{CL}(\gamma_{1^m2^m}) \approx \left(\varphi^o+\gamma_{1^m2^m}\right)\left(-\sigma_{11}+\sigma_{22}\right)+|\tau_{12}|. \tag{100}$$

Solving Eq. (100) depends on the particular form of the constitutive law $\tau = f_{CL}(\gamma)$. For a linear shear behaviour, Eq. (100) was solved by Dávila et al. [5], resulting in

$$\gamma_{1^m2^m} = \frac{\varphi^o G_{12}+|\tau_{12}|}{G_{12}+\sigma_{11}-\sigma_{22}} - \varphi^o. \tag{101}$$

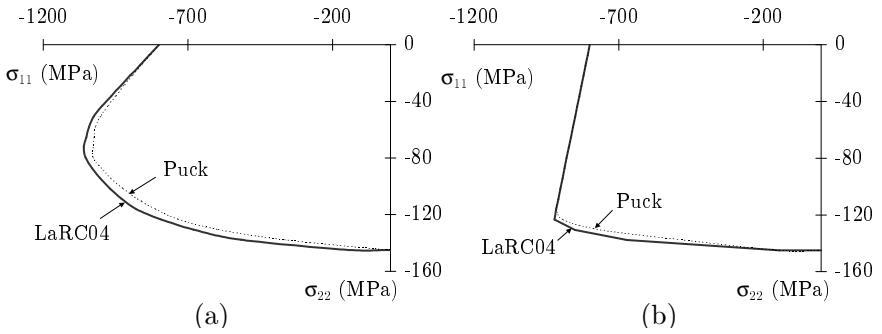

Fig. 12. Failure envelopes for longitudinal compression acting with inplane shear for (a) linear shear behaviour and (b) non-linear shear behaviour

For non-linear shear behaviour, there might be no easy way of solving Eq. (98) or (100) without iterating. Furthermore, Eq. (98) does not always have a solution, since failure by instability is also possible. If, for a specific load state, Eq. (98) does not have a solution (this can be easily checked by plotting the left and right hand side of the equation in a (τ, γ) space), then failure has taken place by instability. The envelope for failure by instability is defined by the system that results from the following two conditions: (i) Eq. (98) is verified; and (ii) the slope (in a (τ, γ) space) of the left hand side of Eq. (98) is the same as the slope of the right hand side. Mathematically, the following system follows,

$$\begin{cases} f_{CL}(\gamma_{1^m2^m}) = -\dfrac{\sigma_{11}-\sigma_{22}}{2}\sin\left(2\left(\varphi^o+\gamma_{1^m2^m}\right)\right)+\left|\tau_{12}\right|\cos\left(2\left(\varphi^o+\gamma_{1^m2^m}\right)\right) \\ \dfrac{\partial f_{CL}(\gamma_{1^m2^m})}{\partial \gamma_{1^m2^m}} = -\left(\sigma_{11}-\sigma_{22}\right)\cos\left(2\left(\varphi^o+\gamma_{1^m2^m}\right)\right)-2\left|\tau_{12}\right|\sin\left(2\left(\varphi^o+\gamma_{1^m2^m}\right)\right). \end{cases} \tag{102}$$

As long as no instability takes place, the misalignment frame can be defined, the stresses can be rotated to that frame, and a matrix failure criterion can be used to check for possible kink-band formation or matrix failure.

Fig. 12 shows the application of this analysis to a biaxial compression in the fiber and matrix direction for a E-glass/DY063 epoxy used in the WWFE [16]. The material properties used are given by Soden et al. [60] and presented in Table 2. For the non-linear behaviour, the experimental data stress vs. strain points given by Soden et al. [60] are used directly by the model (Fig. 13).

Fig. 12(a) shows the different envelopes obtained when using the LaRC04 matrix failure criterion (Eq. (81)) and the Puck matrix failure criterion (Eq. (74)), considering a linear shear behaviour.

Fig. 12(b) presents the application of this failure model for a non-linear shear behaviour (see Eqs. (92) and (98)). Shear non-linearity was not considered explicitly; instead, interpolation and extrapolation was used to get the re-

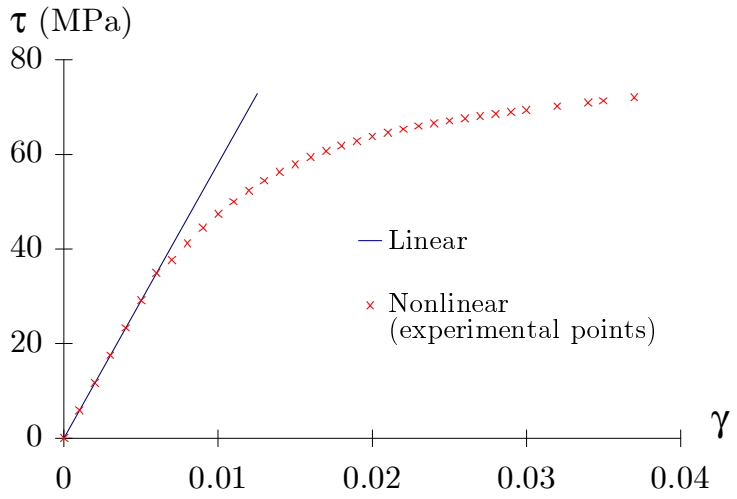

Fig. 13. Linear and non-linear shear curves for an E-glass/DY063 epoxy used in the WWFE, experimental points from Soden et al. [60]

quired information from the experimental data points. The linear and non-linear shear strain vs. shear stress curves are represented in Fig. 13. The effect of the non-linearity on the envelope—Fig. 12(b)—is seen to be considerable, which reinforces the importance of a more comprehensive characterization of composite materials under shear loading.

Note the interesting implications of this model: the failure envelope is dependent on the elastic properties of the material. This is common in fiber compression failure models and in this case reflects the fact that failure takes place in a rotating misalignment frame. Indeed, the magnitude of the rotation of the fibers, $\gamma_{1^m 2^m}$, depends on the shear response.

4.2.2 3D kinking model

The mechanics of kink-band formation is particularly complex. Therefore, a physically-based model that simulates all the details of kink-band formation—initiation, subsequent fiber rotation, fiber fracture at kink-band boundaries, kink-band width, angle, broadening, and that takes into account magnitude, distribution and orientation of initial defects, in-plane shear non-linearity, and all this for a generic 3D stress state—does not seem possible. For the validation of emerging, simplified models, an added difficulty results from the difficulties in obtaining trustworthy experimental data for compression failure under a multiaxial stress state. Consequently, the validation of a specific mechanical model for fiber kinking is bounded to some controversy.

The 2D model for fiber kinking just presented assumes that the initiation of kink-band formation is triggered by matrix failure due to initial fiber misalign-

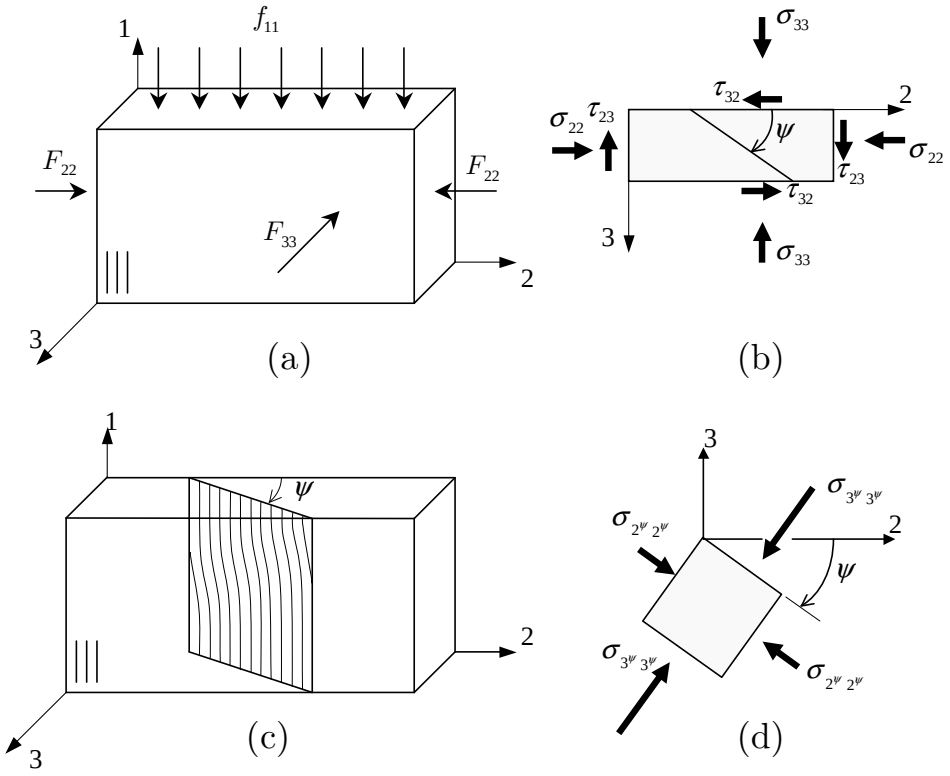

Fig. 14. 3D kinking model

ment. As with most fiber-kinking models, the 2D model assumes that kinking happens in the plane of the lamina.

However, there is significant evidence supporting the importance of 3D analyses for understanding failure by kink-band formation [61,67–71,73–78]. The model that follows generalizes the previous one for a generic 3D stress state.

Consider a unidirectional lamina under compressive stress as shown in Fig. 14(a). The stresses acting on the $(2, 3)$ plane are shown in Fig. 14(b). The kink plane is at an angle ψ with the 2 axis, as shown in Figs. 14(c) and (d). The actual value of the angle ψ depends on the particular stress state [3]. A 2D kinking model assumes that the angle ψ in Fig. 14(c) and (d) is equal to zero. If the composite is constrained so that it cannot move laterally, then the kink plane would have an angle $\psi = 90°$. In general, ψ will have a value between 0 and 180°.

The local stresses in the $(2, 3)$ plane can be found as a function of ψ through the use of transformation equations. For a potential kinking plane oriented at an angle ψ, a negative stress $\sigma_{3^\psi 3^\psi}$ will act as to close microcracks in the

[3] In reality, defects as fiber initial misalignment are not necessarily homogeneously distributed and the kinking plane orientation could in fact also be influenced by a particular distribution

matrix for alternative kinking planes, while a positive $\sigma_{2^\psi 2^\psi}$ will act as to open microcracks thus favouring kinking in that plane. Therefore, the kinking plane is expected to be created at the orientation that maximizes $\sigma_{2^\psi 2^\psi}$ and minimizes $\sigma_{3^\psi 3^\psi}$, which coincide with the local principal directions. Another argument is that the reduced shear stiffness in the kink band would result in fibers rotating in different directions, in case $\tau_{2^\psi 3^\psi}$ was nonzero—however, experimental observations support the contention that kink bands lie in a plane.

With the assumption that the kink plane happens at an angle such that $\tau_{2^\psi 3^\psi} = 0$, the value of the angle ψ that defines the kink plane is given by

$$\tan(2\psi) = \frac{2\tau_{23}}{\sigma_{22} - \sigma_{33}}. \tag{103}$$

The stresses in the kink plane are defined as

$$\begin{cases} \sigma_{2^\psi 2^\psi} = \dfrac{\sigma_{22} + \sigma_{33}}{2} + \dfrac{\sigma_{22} - \sigma_{33}}{2}\cos(2\psi) + \tau_{23}\sin(2\psi) \\ \sigma_{3^\psi 3^\psi} = \sigma_{22} + \sigma_{33} - \sigma_{2^\psi 2^\psi} \\ \tau_{12^\psi} = \tau_{12}\cos(\psi) + \tau_{31}\sin(\psi) \\ \tau_{2^\psi 3^\psi} = 0 \\ \tau_{3^\psi 1} = \tau_{31}\cos(\psi) - \tau_{12}\sin(\psi). \end{cases} \tag{104}$$

After defining the kink plane, the stresses are then rotated to the misalignment frame. This misalignment frame is defined by first determining $\gamma_{1^m 2^m}$ by solving the following equation iteratively:

$$f_{CL}(\gamma_{1^m 2^m}) = -\frac{\sigma_{11} - \sigma_{2^\psi 2^\psi}}{2}\sin\left(2\left(\varphi^o + \gamma_{1^m 2^m}\right)\right) + |\tau_{12^\psi}|\cos\left(2\left(\varphi^o + \gamma_{1^m 2^m}\right)\right). \tag{105}$$

After obtaining $\gamma_{1^m 2^m}$ from Eq. (105), the angle φ is obtained from

$$\varphi = \frac{\tau_{12^\psi}}{|\tau_{12^\psi}|}\left(\varphi^o + \gamma_{1^m 2^m}\right). \tag{106}$$

If Eq. (105) has no solution, then failure has taken place by instability. Otherwise, the misalignment frame is defined and the stresses can be rotated to it to check for matrix failure. In the misalignment frame, the stresses can be

written as

$$\begin{cases} \sigma_{1^m1^m} = \dfrac{\sigma_{11}+\sigma_{2^\psi 2^\psi}}{2} + \dfrac{\sigma_{11}-\sigma_{2^\psi 2^\psi}}{2}\cos(2\varphi) + \tau_{12^\psi}\sin(2\varphi) \\ \sigma_{2^m2^m} = \sigma_{11} + \sigma_{2^\psi 2^\psi} - \sigma_{1^m1^m} \\ \tau_{1^m2^m} = -\dfrac{\sigma_{11}-\sigma_{2^\psi 2^\psi}}{2}\sin(2\varphi) + \tau_{12^\psi}\cos(2\varphi) \\ \tau_{2^m3^\psi} = \tau_{2^\psi 3^\psi}\cos(\varphi) - \tau_{3^\psi 1}\sin(\varphi) \\ \tau_{3^\psi 1^m} = \tau_{3^\psi 1^\psi}\cos(\varphi)\,. \end{cases} \tag{107}$$

The LaRC04 criteria for matrix tension failure, Eq. (40), and matrix compression failure, Eq. (81), can be applied in the misalignment frame to predict failure. The type of failure predicted is matrix failure, and this might or not promote subsequent fiber kinking. While it might be trivial in some cases to predict that subsequent fiber kinking takes place—like for pure compression in the fiber direction, the same is not true for all load combinations.

For $\sigma_{2^m2^m} < 0$, it seems reasonable to assume that failure is by kink-band formation only if Eq. (81) is verified with $\alpha = 0$. Otherwise, the failure is considered to lead to matrix failure, without kink-band formation. Thus, kink-band formation with $\sigma_{2^m2^m} < 0$ is predicted with the criterion

$$\textbf{LaRC04 \#4} \qquad FI_F = \frac{|\tau_{1^m2^m}|}{S^L_{is} - \eta^L\sigma_{2^m2^m}} \leq 1 \tag{108}$$

while matrix failure under biaxial compression is predicted by

$$\textbf{LaRC04 \#5} \qquad FI_M = \left(\frac{\tau^{Tm}}{S^T - \eta^T\sigma^m_n}\right)^2 + \left(\frac{\tau^{Lm}}{S^L - \eta^L\sigma^m_n}\right)^2 \leq 1 \tag{109}$$

with

$$\begin{cases} \sigma^m_n = \dfrac{\sigma_{2^m2^m}+\sigma_{3^\psi 3^\psi}}{2} + \dfrac{\sigma_{2^m2^m}-\sigma_{3^\psi 3^\psi}}{2}\cos(2\alpha) + \tau_{2^m3^\psi}\sin(2\alpha) \\ \tau^{Tm} = -\dfrac{\sigma_{2^m2^m}-\sigma_{3^\psi 3^\psi}}{2}\sin(2\alpha) + \tau_{2^m3^\psi}\cos(2\alpha) \\ \tau^{Lm} = \tau_{1^m2^m}\cos(\alpha) + \tau_{3^\psi 1^m}\sin(\alpha) \end{cases} \tag{110}$$

where the angle α, which is comprised in the interval $]0, \pi[$, is obtained by trying a small number of tentative angles.

For $\sigma_{2^m2^m} \geq 0$, it seems more difficult to agree on a criterion for eventual fiber-kinking after matrix failure, in the absence of experimental data. Possible solutions to identify the conditions triggering fibre-kinking are the use of a threshold value for σ_{11}, or to consider fibre-kinking when the last term of Eq. (40) is equal to 1. Without further support from experimental data, $X^C/2$ is taken here as the threshold value. Thus, for $\sigma_{2^m2^m} \geq 0$ and from Eq. (40),

the criterion for matrix tensile failure under longitudinal compression (with eventual fiber-kinking) is,

LaRC04 #6

$$FI_{M/F} = (1-g)\,\frac{\sigma_{2^m2^m}}{Y_{is}^T} + g\left(\frac{\sigma_{2^m2^m}}{Y_{is}^T}\right)^2 + \\ + \frac{\Lambda_{23}^o \tau_{2^m3^\psi}^2 + \chi\left(\gamma_{1^m2^m}\right)}{\chi\left(\gamma_{12_{is}}^u\right)} \leq 1. \tag{111}$$

5 Applications

5.1 Failure envelope (σ_{22}, τ_{12})

A comparison of results from various failure criteria with the experimental results in the (σ_{22}, τ_{12}) stress plane for an unidirectional composite E-glass/LY556, is shown in Fig. 15. The material properties and test results were reported in the WWFE by Soden et al. [60,86]. The compressive, tensile and shear strengths shown in Table 3 were obtained by averaging the corresponding test data presented in Refs. [60,86]. To apply the Puck tensile matrix failure criterion, it was assumed that $(\partial\tau_{12}/\partial\sigma_{22})|_{\sigma_2=0^-} = (\partial\tau_{12}/\partial\sigma_{22})|_{\sigma_2=0^+}$. The envelopes for Hashin's 1980 criteria and Sun's criteria were calculated using a transverse shear strength obtained from Eq. (68). The friction parameter η^L for Sun's criteria was obtained from Eq. (75) with η^T from Eq. (67).

It can be observed that within the positive range of σ_{22}, all the quadratic failure criteria and LaRC04 give satisfactory results. The most interesting behavior develops when σ_{22} becomes compressive. Hashin's 1973 criterion gives an elliptical envelope with diminishing τ_{12} as the absolute value of compressive σ_{22} increases, while the experimental data shows a definite trend of shear strength increase as σ_{22} goes into compression.

The envelope for Hashin's 1980 criteria provides a modest improvement in accuracy compared to the 1973 criterion. Of the criteria shown in Fig. 15, Sun (Eq. (76)), LaRC04 #2 (Eq. (81)), and Puck (Eq. (74)) capture the shear strength increase at the initial stage of compressive σ_{22}. The results indicate a significant improvement over Hashin's criteria.

Fig. 16 shows the application of LaRC04 for AS4/55A, tested by Swanson et al. [87]. The material properties used are given in Table 3. The predictions for T800/3900-2 composite tested by Swanson et al. [77] are shown in Fig. 17, and the material properties in Table 3.

Table 3
Mechanical properties of E-glass/MY750, from Soden et al. [60,86]

Material	E_{11}	E_{22}	G_{12}	S^L	Y^T	Y^C	α_o
	(GPa)	(GPa)	(GPa)	(MPa)	(MPa)	(MPa)	(°)
E-Glass/LY556	53.48	17.7	5.83	66.5	37.5	130.3	53
AS4/55A	126	11	6.6	51.3	27	91.8	53
T800/3900-2	155	8.5	5.5	100.9	48.8	201.7	53

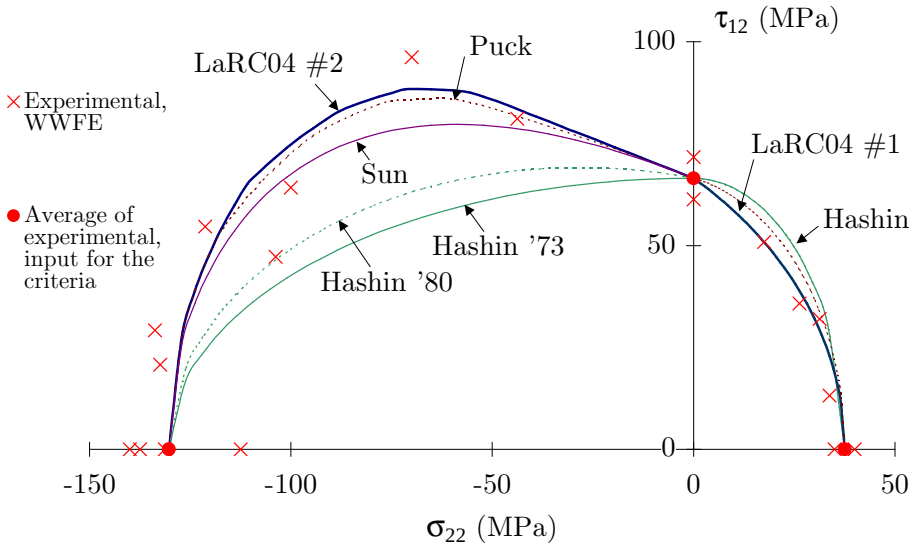

Fig. 15. Failure envelopes and WWFE test data for unidirectional composite E-Glass/LY556

5.2 Failure envelope $(\sigma_{11}, \sigma_{22})$

All of the failure modes represented by the six LaRC04 criteria (Eqs. (40), (81), (82), (108), (109) and (111), and summarized in the Appendix) can be represented as a failure envelope in the (σ_1, σ_2) plane. Testing for biaxial loads presents a number of complexities, and experimental results are rare. However, Waas and Schultheisz [88] report a number of references in which multiaxial compression was studied by superposing a hydrostatic pressure in addition to the compressive axial loading. For all materials considered, there is a significant increase in compressive axial strength with increasing pressure.

As an example, a test case from the WWFE [1] is studied here: the biaxial compression of a 0° E-glass/MY750 epoxy lamina, with material properties given in Table 4. In addition to those properties, the in-plane Poisson's ratio is $\nu_{12} = 0.278$ and the fracture angle for pure in-plane transverse compression is $\alpha_o = 53°$. For the application of the model with non-linear shear behaviour,

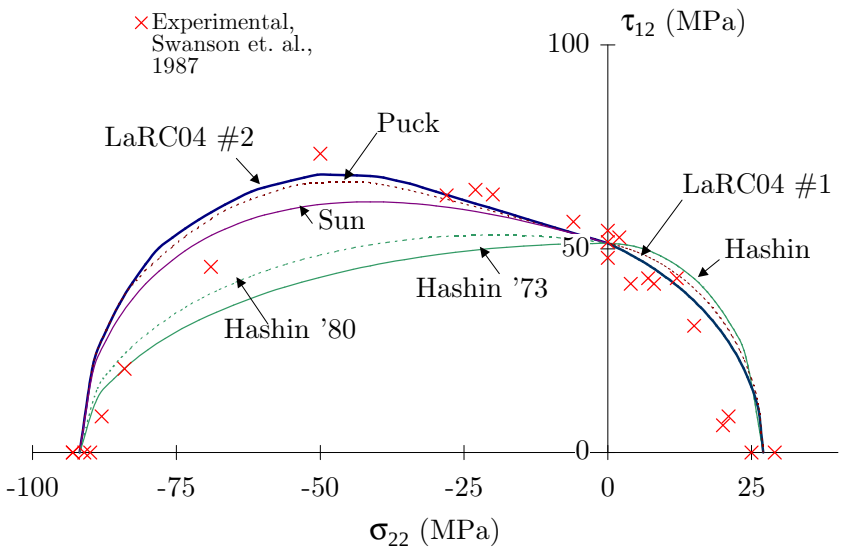

Fig. 16. Failure envelopes and test data from Swanson et al. [87], for an AS4/55A composite

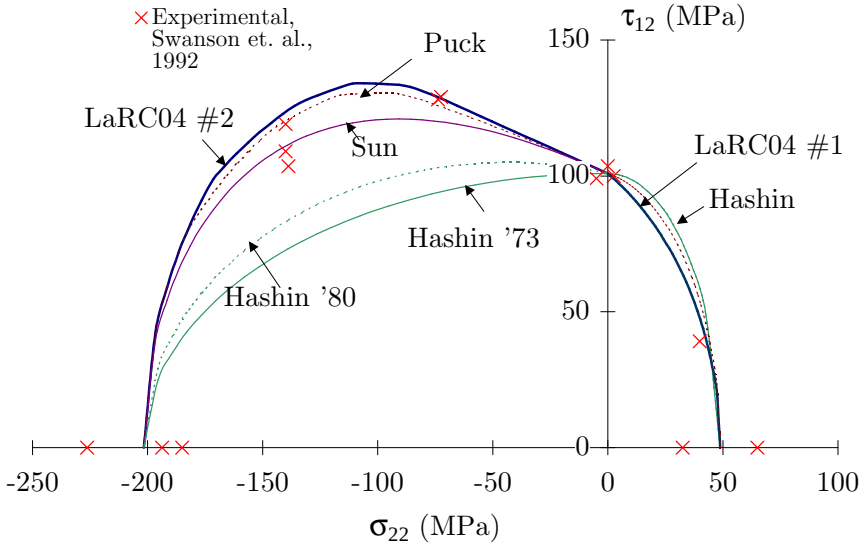

Fig. 17. Failure envelopes and test data from Swanson et al. [77], for an T800/3900-2 composite

the experimental curve given by Soden et al. [60] is used directly. The linear and non-linear shear laws are plotted in Fig. 18(a).

For the LaRC04 3D kinking model, the kinking angle is predicted using Eq. (103). The magnitude of σ_3 is unknown, and depends on the existence of constrains on the 3 direction. Therefore, the 2 roots of Eq. (103) must be considered and are $\psi_1 = 0°$ and $\psi_2 = 90°$, meaning that the kink plane can either be in the plane of the lamina, or in the through-the-thickness direction.

Table 4
Mechanical properties

	Longitudinal		Transverse		Shear
	Tensile	Compression	Tensile	Compression	
Modulus (MPa)	1280	800	40	145	73
Modulus (GPa)	45.6		16.2		5.83

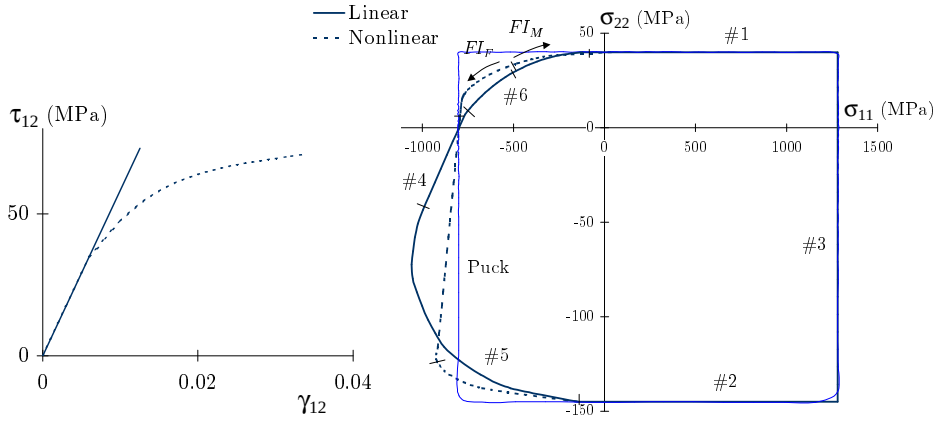

(a) (b)

Fig. 18. (a) Linear and non-linear shear law; (b) biaxial (σ_1, σ_2) failure envelope of 0° E-glass/MY750 epoxy lamina, assuming a kink band in the plane of the lamina

Assuming first that the kink band develops in the plane of the lamina ($\psi = 0^\circ$), either due to the micromechanics of the material or imposed by the testing, the failure envelope comes as in Fig. 18(b). Puck's analysis results, which showed a particularly good correlation with experimental results in the WWFE [1], is also shown for comparison. In the figure, there is good agreement between LaRC04 and Puck in all quadrants except biaxial compression, where LaRC04 predicts—for a kink band developing in the plane of the lamina—an increase of the axial compressive strength with increasing transverse compression.

If it is assumed that the kink band is formed in the through-the-thickness direction (second root of Eq. (103), $\psi = 90^\circ$), the envelope shown in Fig. 19(a) is predicted. If the orientation of the kink plane is unrestricted, the envelope in Fig. 19(b) is obtained.

5.3 Axial compression with superposed hydrostatic pressure

There is not much experimental data on fiber kinking under a multi-axial stress state. One exception is the compressive behaviour of composite rods

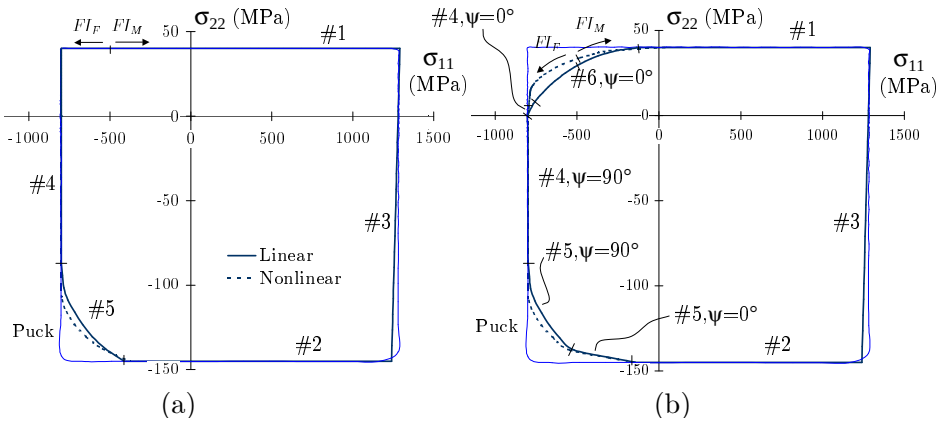

Fig. 19. Biaxial $(\sigma_{11}, \sigma_{22})$ failure envelope of 0° E-glass/MY750 epoxy lamina (a) assuming through-the-thickness kinking; (b) assuming that there are no restrictions to the kinking plane

with superposed hydrostatic pressure [89,90].

Wronsky and Parry [89] made a characterization of the effect of hydrostatic pressure on the compressive strength for a glass fiber reinforced composite. The compressive strength without superposed hydrostatic pressure was measured as 1150 MPa. Three values of shear strength are reported, depending on the test method and specimen dimensions, 42, 48 and 59 MPa. The biggest value of the three is used herein, because it is expected to be the most representative of the three. These material properties are not sufficient to completely define the material. Therefore, some material properties have to be assumed from their typical values. The shear modulus is 6.6 GPa, the fracture angle in matrix compression is $\alpha_o = 53°$, and the transverse compressive strength is 140 MPa. Linear and a non-linear approximations of the material's shear response are shown in Fig. 20(a). The non-linear curve uses the logarithmic [4] function $\tau = k_1 \ln(k_2\gamma + 1)$, with $k_1 = 200$ MPa and $k_2 = 33$, which yields the correct initial shear modulus, $G_{12} = k_1 k_2 = 6.6$ GPa, and matches particularly well the experimental points, as shown in Fig. 20(b). The same figure shows that, considering a linear shear model, the global trend is captured, but an over-prediction of the axial strength results for the higher values of superposed hydrostatic pressure.

Parry and Wronsky [90] compressed 8 mm carbon-epoxy rods for several values of superposed hydrostatic pressure. Three values of compressive strength at atmospheric pressure are reported (depending on the test specimen's batch and its shape): 1.3 MPa, 1.33 MPa and 1.5 MPa. The corresponding average is considered here. The shear strength reported is 75 MPa. As before, some material properties have to be assumed to apply the present model. The shear

[4] A logarithmic function is used because, while correctly representing the shear non-linear behaviour of composites, it can be easily inverted

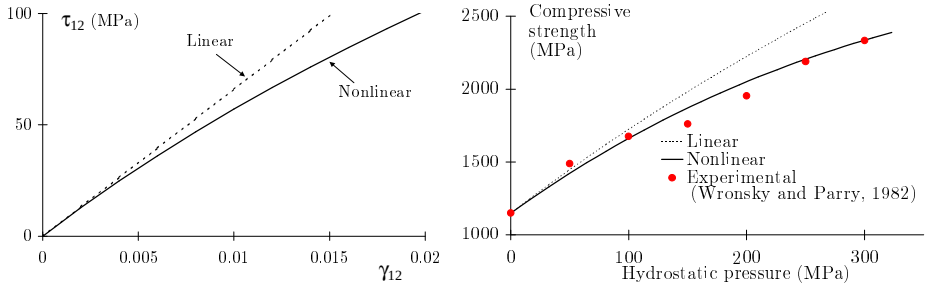

Fig. 20. Test case corresponding to Wronsky and Parry's [89] experiments (a) linear and non-linear shear curves considered; (b) compressive strength as a function of the hydrostatic pressure

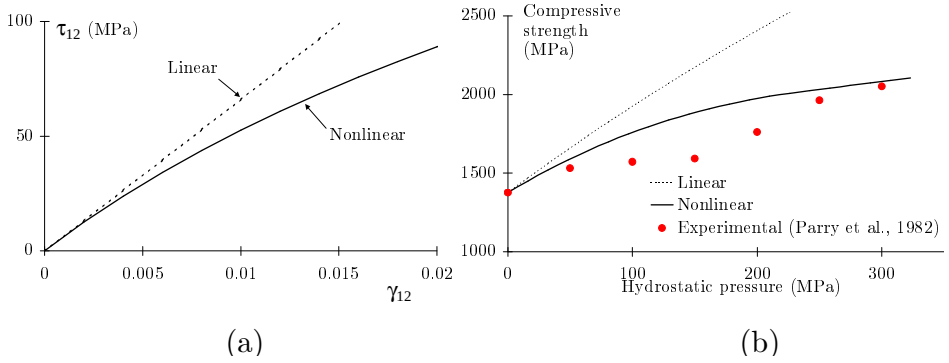

Fig. 21. Test case corresponding to Parry and Wronsky's [90] experiments (a) linear and non-linear shear curves considered; (b) compressive strength as a function of the hydrostatic pressure

modulus is 6.6 GPa, the fracture angle in matrix compression is $\alpha_o = 53°$, the transverse compressive strength is 170 MPa. The predictions for a linear shear model (Fig. 21(a)) are shown in Fig. 21(b). The effect of shear non-linearity is the same as for the previous example. Considering the non-linear stress vs. strain curve in Fig. 21(a) (logarithmic curve, $\tau = k_1 \ln(k_2\gamma + 1)$, with $k_1 = 120$ MPa and $k_2 = 55$, which yields the same initial shear modulus), the predictions in Fig. 21(b) are in good agreement with the experimental points.

The comparison of experimental results and predictions in Figs. 20 and 21 suggests that the physics of the compressive behaviour is captured by the kinking model.

5.4 Cross-ply laminates

Shuart [73] studied the compression failure of $[\pm\theta]_s$ laminates and found that for $\theta < 15°$, the dominant failure mode in these laminates is interlaminar shearing; for $15° < \theta < 50°$, it is in-plane matrix shearing; and for $\theta > 50°$, it

Table 5
Material properties of AS4/3502

E_{11}	E_{22}	G_{12}	ν_{12}	S_{is}^{L}	Y^{C}	X^{C}
(GPa)	(GPa)	(GPa)		(MPa)	(MPa)	(MPa)
127.6	11.3	6.0	0.3	95.1	255	1045

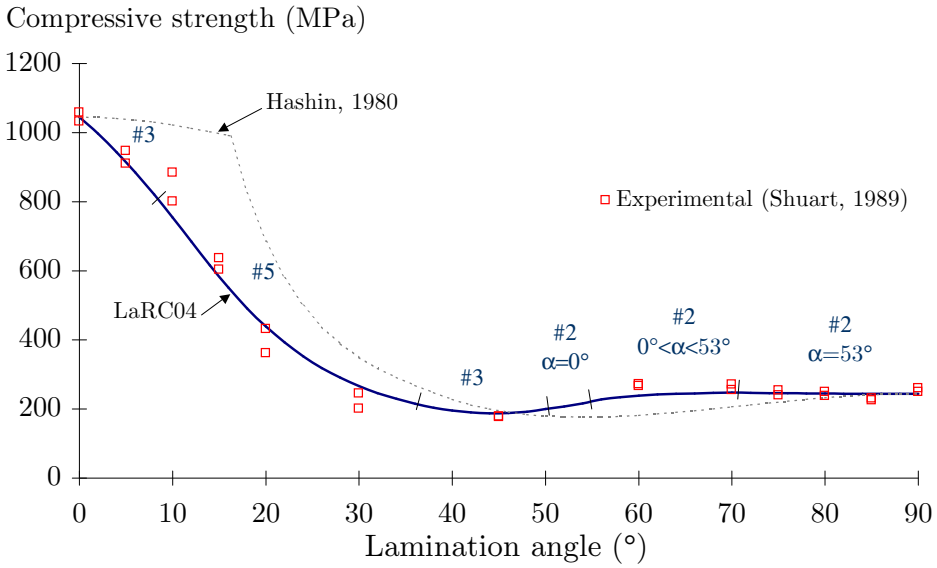

Fig. 22. Compressive strength as a function of ply orientation for AS4-3502 $[\pm\theta]_s$ laminates

is matrix compression. Fiber scissoring due to matrix material non-linearity caused the switch in failure mode from in-plane matrix shearing to matrix compression failure at larger lamination angles. The material properties used for the analysis are given by Shuart [73] and shown in Table 5. Further to those properties, the fracture angle in pure transverse compression is considered to be $\alpha_o = 53°$.

The results shown in Fig. 22 indicate that the predicted strengths using LaRC04 criteria correlate well with the experimental results. The compressive strength predicted using Hashin's 1980 criteria is also shown in Fig. 22. For $\theta < 20°$, the Hashin criterion for fiber compression results in an over-prediction of the failure load because the criterion does not account for the effect of in-plane shear on fiber failure. For lamination angles near 70°, the use of the Hashin criteria result in an under-prediction of the failure load because the criteria do not account for the increase in shear strength caused by transverse compression. All of these effects are correctly captured by the LaRC04 criteria, which results in a good correlation between the calculated and experimental values.

6 Conclusions

Material models based on the physics of failure can yield criteria that succeed in predicting failure under a broad range of load combinations. Considering the current difficulties in accurately predicting failure [1], the ability of physically-based models to capture the physics of the failure process and correctly predict failure envelopes is particularly significant and should encourage further research. In this paper, physically-based models of the different failure modes result in a set of six physically-based failure criteria devoid of empirical variables—the LaRC04 criteria—that can be used directly by the designer. A few considerations on the models presented are now discussed; some of them will be the focus of further work.

Non-linear shear behaviour is an important factor affecting strength in a general loading situation. Furthermore, it is known that the shear behaviour depends on the stress in the in-plane transverse direction (the shear response gets "stiffer" with compressive transverse stresses [6]). In the future, it would be desirable to consider the dependence of the shear stress on eventual superposed transverse stress. Furthermore, the shear strength reported in the literature is often the shear stress at some strain level—as recommended by actual standard methods [91]. Although convenient for design purposes, this value of the shear stress has no direct correspondence with failure and is meaningless for physically-based failure models.

For fiber kinking, only matrix failure (as well as some form of instability) is assumed to trigger the failure. This consideration is believed to be accurate for carbon-reinforced composites. However, a more general model that includes the possibility of fiber buckling, as well as fiber failure itself would be desirable. Furthermore, the strength in a generic loading situation is very sensitive to the initial fiber misalignment angle. However, this misalignment angle results from manufacturing limitations, and should be expected to be different for panels or components with different dimensions and geometry. Therefore, the value measured using standard compression specimens could not be representative for other more complex components. Finally, residual stresses—present in the compression specimens—affect the value measured of the fiber misalignment angle. In more complex components, the residual stresses will certainly be different, and relax over time, which restricts the applicability of the proposed model, and should be addressed in the future.

Acknowledgements

The first author whishes to acknowledge the funding from the Portuguese

Foundation for Science and Technology.

References

[1] M. J. Hinton, P. G. Soden, A comparison of the predictive capabilities of current failure theories for composite laminates, judged against experimental evidence, Composites Science and Technology 62 (2002) 1725–1797.

[2] P. P. Camanho, C. G. Dávila, M. F. de Moura, Numerical simulation of mixed-mode progressive delamination in composite materials, Journal of Composite Materials 37 (16) (2003) 1415–1438.

[3] A. Turon, P. P. Camanho, J. Costa, C. G. Dávila, An interface damage model for the simulation of delamination under variable-mode ratio in composite materials, Tech. Rep. NASA/TM-2004-213277, National Aeronautics and Space Administration, U. S. A. (2004).

[4] ABAQUS Users Manual Version 6.1, Hibbit, Karlsson and Sorensen Inc. (2000).

[5] C. G. Dávila, P. P. Camanho, Failure criteria for FRP laminates in plane stress, Tech. Rep. NASA/TM-2003-212663, National Aeronautics and Space Administration, U. S. A. (2003).

[6] A. Puck, H. Schürmann, Failure analysis of FRP laminates by means of physically based phenomenological models, Composites Science and Technology 58 (1998) 1045–1067.

[7] A. S. Argon, Fracture of composites, in: Treatise on Materials Science and Technology, Academic Press, New York, 1972, pp. 79–114.

[8] C. G. Dávila, N. Jaunky, S. Goswami, Failure criteria for FRP laminates in plane stress, in: 44th AIAA/ ASME/ ASCE/ AHS/ ASC Structures, Structural Dynamics, and Materials Conference, 2003, AIAA Paper 2003-1991.

[9] G. J. Dvorak, N. Laws, Analysis of progressive matrix cracking in composite laminates II. First ply failure, Journal of Composite Materials 21 (1987) 309–329.

[10] F. Paris, A study of failure criteria of fibrous composite materials, Tech. Rep. NASA/CR-2001-210661, National Aeronautics and Space Agency (2001).

[11] Z. Hashin, A. Rotem, A fatigue failure criterion for fibre reinforced materials, Journal of Composite Materials 7 (1973) 448–464.

[12] Z. Hashin, Failure criteria for unidirectional fibre composites, Journal of Applied Mechanics 47 (1980) 329–334.

[13] A. Puck, Calculating the strength of glass fibre/plastic laminates under combined load, Kunststoffe, German Plastics 55 (1969) 18–19, original in German.

[14] A. Puck, W. Schneider, On failure mechanisms and failure criteria of filament-wound glass-fibre/resin composites, Plastics and Polymers (1969) 33–44.

[15] I. Shahid, F. K. Chang, An accumulative damage model for tensile and shear failures of laminated composite plates, Journal of Composite Materials 29 (1995) 926–981.

[16] M. J. Hinton, P. G. Soden, Predicting failure in composite laminates: the background to the exercise, Composites Science and Technology 58 (1998) 1001–1010.

[17] L. J. Hart-Smith, Prediction of the original and truncated maximum-strain failure models for certain fibrous composite laminates, Composites Science and Technology 58 (7) (1998) 1151–1178.

[18] L. J. Hart-Smith, Predictions of a generalized maximum-shear-stress failure criterion for certain fibrous composite laminates, Composites Science and Technology 58 (7) (1998) 1179–1208.

[19] P. K. Gotsis, C. C. Chamis, L. Minnetyan, Prediction of composite laminate fracture: micromechanics and progressive fracture, Composites Science and Technology 58 (7) (1998) 1137–1149.

[20] L. N. McCartney, Predicting transverse crack formation in cross-ply laminates, Composites Science and Technology 58 (7) (1998) 1069–1081.

[21] A. Rotem, Prediction of laminate failure with the rotem failure criterion, Composites Science and Technology 58 (7) (1998) 1083–1094.

[22] C. T. Sun, J. Tao, Prediction of failure envelopes and stress/strain behaviour of composite laminates, Composites Science and technology 58 (7) (1998) 1125–1136.

[23] C. T. Sun, B. J. Quinn, D. W. Oplinger, Comparative evaluation of failure analysis methods for composite laminates, DOT/FAA/AR (1996) 95–109.

[24] K.-S. Liu, S. W. Tsai, A progressive quadratic failure criterion for a laminate, Composites Science and Technology 58 (7) (1998) 1023–1032.

[25] S. W. Tsai, E. M. Wu, A general theory of strength for anisotropic materials, Journal of Composite Materials 5 (1971) 58–80.

[26] W. E. Wolfe, A strain-energy based failure criterion for non-linear analysis of composite laminates subjected to biaxial loading, Composites Science and Technology 58 (7) (1998) 1107–1124.

[27] E. C. Edge, Stress-based grant-sanders method for predicting failure of composite laminates, Composites Science and Technology 58 (7) (1998) 1033–1041.

[28] P. A. Zinoviev, S. V. Grigoriev, O. V. Lebedeva, L. P. Tairova, The strength of multilayered composites under a plane-stress state, Composites Science and Technology 58 (7) (1998) 1209–1223.

[29] N. Laws, A note on interaction energies associated with cracks in anisotropic solids, Philosophical Magazine 36 (2) (1977) 367–372.

[30] J. D. Eshelby, The determination of the elastic field of an ellipsoidal inclusion, and related problems, Proceedings of the Royal Society A 241 (1957) 376–396.

[31] N. Kinoshita, T. Mura, Elastic fields of inclusions in anisotropic media, Physica Status Solidi: A 5 (1971) 759–768.

[32] G. Faivre, Hétérogénéités ellipsoïdales dans un milieu élastique anisotrope, Le Journal de Physique 32 (1971) 325–331.

[33] A. Parvizi, K. Garrett, J. Bailey, Constrained cracking in glass fibre-reinforced epoxy cross-ply laminates, Journal of Material Science 13 (1978) 195–201.

[34] A. S. D. Wang, Fracture mechanics of sublaminate cracks in composite materials, Composites Technology Review 6 (2) (1984) 45–62.

[35] S. C. Tan, R. J. Nuismer, A theory for progressive matrix cracking in composite laminates, Journal of Composite Materials 23 (1989) 1029–1047.

[36] R. Talreja, Transverse cracking and stiffness redction in composite laminates, Journal of Composite Materials 19 (1985) 355–375.

[37] D. H. Allen, C. E. Harris, S. E. Groves, A thermomechanical constitutive theory for elastic composites with distributed damage- I. theoretical developments, International Journal of Solids and Structures 23 (9) (1987) 1301–1318.

[38] D. H. Allen, C. E. Harris, S. E. Groves, A thermomecanical constitutive theory for elastic coposites with distributed damage- II. application to matrix cracking in laminated composites, International Journal of Solids and Structures 23 (9) (1987) 1319–1338.

[39] R. Talreja, S. Yalvac, L. D. Yats, D. G. Wetters, Transverse cracking and stiffness reduction in cross ply laminates of different matrix toughness, Journal of Composite Materials 26 (11) (1992) 1644–1663.

[40] F. K. Chang, M. H. Chen, The in situ ply shear strength distributions in graphite/epoxy laminated composites, Journal of Composite Materials 21 (1987) 708–733.

[41] D. L. Flaggs, K. M. H, Experimental determination of the in situ transverse lamina strength in graphite/epoxy laminates, Journal of Composite Materials 16 (1982) 103–116.

[42] N. Laws, G. J. Dvorak, Progressive transverse cracking in composite laminates, Journal of Composite Materials 22 (1988) 900–919.

[43] J. Li, J. K. Sen, Analysis of frame-to-skin joint pull-off tests and prediction of the delamination failure, in: 42nd AIAA/ASME/ASCE/AHS/ASC Structures, Structural Dynamics and Materials Conference, Seattle, WA, USA, 2000.

[44] J. Li, Three-dimensional effects in the prediction of flange delamination in composite skin-stringer pull-off specimens, in: 15th Conference of the American Society for Composites, Texas, USA, 2000.

[45] H. T. Hahn, T. Johannesson, Fracture of unidirectional composites: Theory and applications, in: G. J. Dvorak (Ed.), Mechanics of Composite Materials, AMD, 1983, pp. 135–142.

[46] E. M. Wu, R. C. J. Reuter, Crack extension in fiberglass reinforced plastics and a critical examination of the general fracture criterion. theoretical and applyed mechanics report no. 275, University of Illinois (1965).

[47] R. S. Sandhu, Nonlinear response of unidirectional and angle-ply laminates, in: AIAA Paper No. 74-380, 15th AIAA-ASME Structural Dynamics and Materials Conference, Las Vegas, Nevada, 1974.

[48] F.-K. Chang, R. A. Scott, Failure strength of nonlinearly elastic composite laminates containing a pin loaded hole, Journal of Composite Materials 18 (1984) 464–477.

[49] H. Tada, P. C. Paris, G. R. Irwin, The Stress Analysis of Cracks Handbook, 3rd. Ed., Americal society of Mechanical Engineers, New York, 2000.

[50] H. T. Hahan, S. W. Tsai, Nonlinear elastic behavior of unidirectional composite laminae, Journal of Composite Materials 7 (1973) 102–118.

[51] D. Leguillon, Strength or toughness? A criterion for crack onset at a notch, European Journal of Mechanics - A/Solids 21 (1) (2002) 61–72.

[52] A. Puck, H. Schürmann, Failure analysis of FRP laminates by means of physically based phenomenological models, Composites Science and Technology 62 (2002) 1633–1662.

[53] R. M. Christensen, S. J. de Teresa, Failure plane orientations for transverse loading of a unidirectional fiber composite, International Journal of Solids and Structures 40 (25) (2003) 7055–7062.

[54] S. Kawabata, Strength of epoxy resin under multiaxial stress field, in: Proceedings of the ICCM-IV, Tokyo, 1982, pp. 191–168.

[55] J. P. Boehler, J. Raclin, Failure criteria for glass-fiber reinforced composites under confining pressure, Journal of Structural Mechanics 13 (3-4) (1985) 371–392.

[56] A. Taliercio, P. Sagramoso, Uniaxial strength of polymeric-matrix fibrous composites predicted through a homogenization approach, International Journal of Solids and Structures 32 (14) (1995) 2095–2123.

[57] L. DiLandro, M. Pegoraro, Carbon fibre-thermoplastic matrix adhesion, Journal of Material Science 22 (1987) 1980–1986.

[58] M. C. Larson, H. F. Miles, On the effects of friction, roughness and toughness on interfacial sliding in brittle composites, Mechanics of Materials 27 (2) (1998) 77–89.

[59] S. T. Pinho, L. Iannucci, P. Robinson, Physically-based failure models and criteria for laminated fibre-reinforced composites. Part I: Development, Submitted to Composites: Part A (2004).

[60] P. D. Soden, M. J. Hinton, A. S. Kaddour, Lamina properties, lay-up configurations and loading conditions for a range of fibre-reinforced composite laminates, Composites Science and Technology 58 (1998) 1011–1022.

[61] C. R. Schultheisz, A. M. Waas, Compressive failure of composites, part I: Testing and micromechanical theories, Progress in Aerospace Sciences 32 (1996) 1–42.

[62] V. W. Rosen, Mechanics of composite strengthening, Fiber Composite Materials American Society of Metals, Metals Park, Ohio (1965) 37–75.

[63] H. Schuerch, Prediction of compressive strength in uniaxial boron fiber-metal matrix composite materials, AIAA Journal 4 (1) (1966) 102–106.

[64] L. B. Greszczuk, Microbuckling of unidirectional composites, Tech. Rep. Air Force Materials Laboratory Technical Report, OHAFML-TR-71-231, Wright-Patterson Air Force Base, OH (1972).

[65] L. B. Greszczuk, Failure mechanics of composites subjected to compressive loading, Tech. Rep. Air Force Materials Laboratory Technical Report, AFML-TR-72-107, Wright-Patterson Air Force Base, OH (1972).

[66] L. B. Greszczuk, Microbuckling of lamina reinforced composites, in: Composite materials: Testing and Design (Third Conference), ASTM STP 546, American Society for Testing and Materials, Philadelphia, 1974, pp. 5–29.

[67] L. B. Greszczuk, Microbuckling failure of circular fiber-reinforced composites, AIAA Journal 13 (10) (1975) 1311–1318.

[68] J. R. Lager, R. R. June, Compressive strength of boron-epoxy composites, Journal of Composite Materials 3 (1969) 48–56.

[69] M. E. de Ferran, B. Harris, Compression strength of polyester resin reinforced with steel wires, Journal of Composite Materials 4 (1970) 62–72.

[70] D. Purslow, R. T. Potter, The effect of environment on the compression strength of notched CFRP / a fractografic investigation, Composites 15 (2) (1984) 112–120.

[71] A. M. Waas, C. D. J. Babcock, W. G. Knauss, An experimental study of compression failure of fibrous laminated composites in the presence of stress gradients, International Journal of Solids and Structures 26 (9-10) (1990) 1071–1098.

[72] J. G. Davis Jr, Compressive strength of fiber-reinforced composite materials, in: Composite Reliability, ASTM STP 580, Americal Society for Testing and Materials, Philadelphia, 1975, pp. 364–377.

[73] M. J. Shuart, Failure of compression-loaded multidirectional composite laminates, AIAA Journal 27 (1989) 1274–1279.

[74] M. J. Shuart, Short-wavelength buckling and shear failures for compression-loaded composite laminates, Tech. Rep. NASA Technical Memorandum, TM-87640, NASA (1985).

[75] J. C. Grandidier, M. Potier-Ferry, Microbuckling and homogenization for long fiber composites, Zeitschrift fur Angewandte Mathematik und Mechanik 71 (4) (1991) T371–T374.

[76] A. Agah-Tehrani, S. Gunawardena, Micro- and macrobifurcation of fibrous metal-matrix composites under uniaxial compression, Journal of the Mechanics and Physics of Solids 39 (1991) 1073–1103.

[77] S. R. Swanson, A micro-mechanical model for in-situ compression strength of fiber composite laminates, Transactions of the American Society of Mechanical Engineers. Series H, Journal of Engineering Materials and Technology 114 (1992) 8–12.

[78] I. G. Tadjbakhsh, Y. M. Wang, Fiber buckling in three-dimensional periodic-array composites, International Journal of Solids and Structures 29 (1992) 3169–3183.

[79] C. R. Chaplin, Compressive fracture in unidirectional glass-reinforced plastics, Journal of Materials Science 12 (1977) 347–352.

[80] R. R. Effendi, J. J. Barrau, D. Guedra-Degeorges, Failure mechanism analysis under compression loading of unidirectional carbon/epoxy composites using micromechanical modelling, Composite Structures 31 (2) (1995) 87–98.

[81] H. T. Hahn, M. M. Sohi, Buckling of a fiber bundle embedded in epoxy, Composites Science and Technology 27 (1986) 25–41.

[82] M. R. Piggott, B. Harris, Compression strength of carbon, glass and kevlar-49 fibre reinforced polyester resins, Journal of Materials Science 15 (1980) 2523–2538.

[83] M. R. Piggott, A theoretical framework for the compressive properties of aligned fibre composites, Journal of Materials Science 16 (1981) 2837–2845.

[84] B. Budiansky, Micromechanics, Computers and Structures 16 (1983) 3–12.

[85] B. Budiansky, N. A. Fleck, Compressive failure of fibre composites, Journal of the Mechanics and Physics of Solids 41 (1) (1993) 183–211.

[86] P. D. Soden, M. J. Hinton, A. S. Kaddour, Biaxial test results for strength and deformation of a range of e-glass and carbon fibre reinforced composite laminates: Failure exercise benchmark data, Composites Science and Technology 62 (2002) 1489–1514.

[87] S. R. Swanson, M. J. Messick, Z. Tian, Failure of Carbon/Epoxy lamina under combined stress, Journal of Composite Materials 21 (1987) 619–630.

[88] A. M. Waas, C. R. Schultheisz, Compressive failure of composites, part II: experimental studies, Progress in Aerospace Sciences 32 (1996) 43–78.

[89] A. S. Wronsky, T. V. Parry, Compressive failure and kinking in uniaxially aligned glass-resin composite under superposed hydrostatic pressure, Journal of Materials Science 17 (1982) 3656–3662.

[90] T. V. Parry, A. S. Wronsky, Kinking and compressive failure in uniaxially aligned carbon fibre composite tested under superposed hydrostatic pressure, Journal of Materials Science 17 (1982) 893–900.

[91] ASTM Standard D3518/D3518M(2001), Standard test method for in-plane shear reponse of polymer matrix composite materials by tensile test of a +/-45 laminate (2001).

[92] R. S. Rivlin, A. G. Thomas, Rupture of rubber. I. Characteristic energy for tearing, Journal of Polymer Science 10 (1953) 291–318.

Appendix - Pragmatic solution for the critical energy release rates for non-linear shear behaviour

Introduction

Consider a generic solid made of a linear elastic material with an initial crack—Fig. 23(a). Let the crack grow by an area ∂A. The energy absorbed by the solid to create the surface of area ∂A is ∂W_s. Neglecting thermal effects, energy balance requires ∂W_s to be equal to the energy transferred to the body through external work, ∂F, minus the change in strain energy ∂U of the body, i.e.,

$$\partial W_s = \partial F - \partial U. \tag{112}$$

By definition of energy release rate G, it follows that

$$G = \frac{\partial W_s}{\partial A} = \frac{\partial F - \partial U}{\partial A} = -\frac{\partial \Pi}{\partial A} \tag{113}$$

where Π is the potential energy defined as $\Pi = U - F$.

Considering the diagram in Fig. 23(b), it can be concluded that

$$\partial U = \frac{1}{2}\left(P + \partial P\right)\left(\Delta + \partial \Delta\right) - \frac{1}{2} P \Delta \tag{114}$$

and

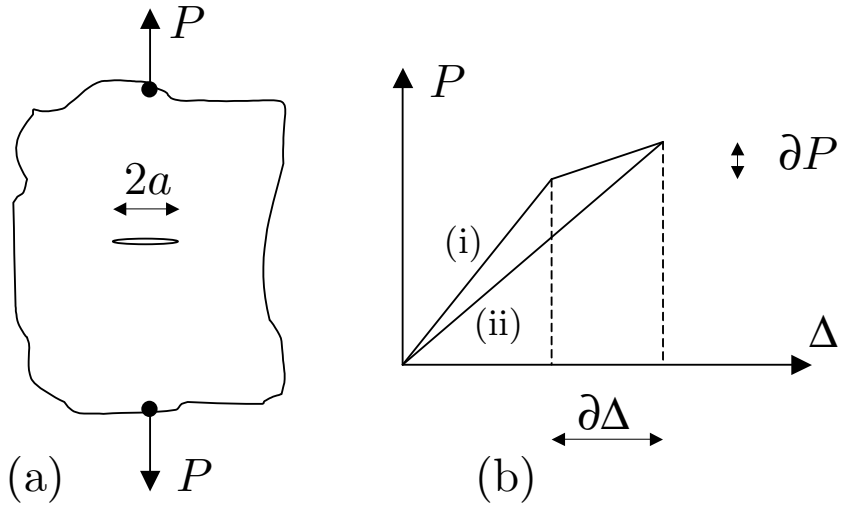

Fig. 23. (a) Generic cracked body being loaded; (b) load displacement curve corresponding to a crack length $2a$ (i) and $2\left(a + \partial a\right)$ (ii)

$$\partial F = P\partial\Delta + \frac{1}{2}\partial P\partial\Delta = \left(P + \frac{\partial P}{2}\right)\partial\Delta \tag{115}$$

Thus,

$$\partial\left(F - U\right) = \frac{1}{2}\left(P\partial\Delta - \Delta\partial P\right) \tag{116}$$

and the critical energy release rate is expressed as

$$G = \frac{1}{2}\left(P\frac{\partial\Delta}{\partial A} - \frac{\partial P}{\partial A}\right) = \frac{1}{2b}\left(P\frac{\partial\Delta}{\partial a} - \frac{\partial P}{\partial a}\right) \tag{117}$$

where b is the thickness of the solid and a is the crack length. Defining the compliance C of the cracked body as

$$C = \frac{\Delta}{P} \tag{118}$$

it follows that

$$\partial\Delta = P\partial C + C\partial P \tag{119}$$

and, designating the load at onset of crack propagation as P_c, the critical energy release rate is

$$G_c = \frac{P_c^2}{2b}\frac{\partial C}{\partial a}. \tag{120}$$

Non-linear in-plane shear behaviour

Considering the energy release rate given by Eq. (113), but carrying the differentiation at constant displacement of the load application-points, hence with no work done by the external forces, it follows, at onset of crack propagation,

$$-\left(\frac{\partial U}{\partial A}\right) = G_c. \tag{121}$$

Following the approach first proposed by Rivlin and Thomas [92], the assumption is made that the presence of a crack in a body will reduce the strain-energy density to zero over a well-defined volume V, and will not affect it outside that area. Let the uniform strain density of the uncracked body be

$$W_o = \int_0^{\varepsilon_{ij}} \sigma_{ij} d\varepsilon_{ij} \tag{122}$$

and for the particular case of pure in-plane shear loading

$$W_o = \int_0^{\gamma_{12}} \tau_{12} d\gamma_{12}. \tag{123}$$

The loss in strain energy due to the presence of the crack is

$$-\left(U-U_o\right)=W_oV=\frac{1}{2}\chi\left(\gamma_{12}\right)V \tag{124}$$

where

$$\chi\left(\gamma_{12}^u\right)=2\int_0^{\gamma_{12}}\tau_{12}d\gamma_{12} \tag{125}$$

and U_o is the strain energy of the body for the situation without a crack. The critical energy release rate is

$$G_{IIc}=\frac{1}{2}\chi\left(\gamma_{12}^u\right)\frac{\partial V}{\partial A}. \tag{126}$$

Consider first the situation where the elliptical crack grows in the transversal direction. The area of the crack is proportional to a_oa_L and thus

$$\partial A\propto a_L\partial a_o. \tag{127}$$

The volume where the strain energy density is reduced to zero due to the crack can be assumed to be proportional to $a_o^2a_L$ and thus

$$\partial V\propto a_oa_L\partial a_o. \tag{128}$$

It follows from Eqs. 127 and 128 that

$$\frac{\partial V}{\partial A}\propto a_o. \tag{129}$$

In order to recast Dvorak and Laws's solution for linear elastic materials [9], the constant of proportionality in Eq. 129 has to be π. Thus, the expression for $G_{IIc}(T)$ results:

$$G_{IIc}(T)=\frac{\pi a_o}{2}\chi\left(\gamma_{12}^u\right). \tag{130}$$

Proceeding in the same way for propagation in the longitudinal direction, the following expression results:

$$G_{IIc}(L)=\frac{\pi a_o}{4}\chi\left(\gamma_{12}^u\right). \tag{131}$$

Appendix - Summary of LaRC04 failure criteria

The LaRC04 criteria is summarized in Table 6. The required unidirectional material properties for the criteria are: E_{11}, E_{22}, G_{12}, ν_{12}, X^T, X^C, Y^T, Y^C, S^L, G_{Ic}, G_{IIc}. The following optional properties may be provided: η^L, α_o. The expressions needed to obtain the parameters used in in Table 6 are given in following sub-sections.

Expressions for matrix tensile failure

The in-situ strength values for thick embedded plies are

$$\begin{aligned} Y_{is}^T &= 1.12\sqrt{2}Y^T \quad \text{and} \\ \gamma_{12is}^u &= \chi^{-1}\left[2\chi\left(\gamma_{12}^u\right)\right]. \end{aligned} \tag{132}$$

The in-situ strengths for thin embedded plies are:

$$\begin{aligned} Y_{is}^T &= \sqrt{\frac{8G_{Ic}}{\pi t \Lambda_{22}^o}} \\ \gamma_{12is}^u &= \chi^{-1}\left(\frac{8G_{IIc}}{\pi t}\right) \end{aligned} \qquad \text{where} \quad \Lambda_{22}^o = 2\left(\frac{1}{E_{22}} - \frac{\nu_{21}^2}{E_{11}}\right). \tag{133}$$

The toughness ratio g is obtained from fracture mechanics test data or from the unidirectional properties. For a thin embedded ply,

$$g = \frac{G_{Ic}}{G_{IIc}}, \tag{134}$$

otherwise, g can be obtain from either of the following expressions:

$$g = 1.12^2 \frac{\Lambda_{22}^o \left(Y^T\right)^2}{\chi\left(\gamma_{12}^u\right)}. \tag{135}$$

Table 6
Summary of the LaRC04 criteria

MATRIX FAILURE

Matrix tensile failure $\sigma_{22} \geq 0$	**Matrix compressive failure** $\sigma_{22} < 0$	
LaRC #1	$\sigma_{11} < -Y^C$ LaRC #5	$\sigma_{11} \geq -Y^C$ LaRC #2
$FI_M = (1-g)\frac{\sigma_2}{Y_{is}^T} + g\left(\frac{\sigma_2}{Y_{is}^T}\right)^2 + \frac{\Lambda_{23}^o \tau_{23}^2 + \chi(\gamma_{12})}{\chi\left(\gamma_{12is}^u\right)}$	$FI_M = \left(\frac{\tau^{Tm}}{S^T - \eta^T \sigma_n^m}\right)^2 + \left(\frac{\tau^{Lm}}{S_{is}^L - \eta^L \sigma_n^m}\right)^2$	$FI_M = \left(\frac{\tau^T}{S^T - \eta^T \sigma_n}\right)^2 + \left(\frac{\tau^L}{S_{is}^L - \eta^L \sigma_n}\right)^2$

FIBER FAILURE

Fiber tensile failure $\sigma_{11} \geq 0$	**Fiber compressive failure** $\sigma_{11} < 0$	
LaRC #3	$\sigma_{2^m 2^m} < 0$ LaRC #4	$\sigma_{2^m 2^m} \geq 0$ LaRC #6
$FI_F = \frac{\sigma_{11}}{X^T}$	$FI_F = \left(\frac{\tau_{1^m 2^m}}{S_{is}^L - \eta^L \sigma_{2^m 2^m}}\right)^2$	$FI_{M/F} = (1-g)\frac{\sigma_{2^m 2^m}}{Y_{is}^T} + g\left(\frac{\sigma_{2^m 2^m}}{Y_{is}^T}\right)^2 + \frac{\Lambda_{23}^o \tau_{2^m 3^\psi}^2 + \chi(\gamma_{1^m 2^m})}{\chi\left(\gamma_{12is}^u\right)}$

Expressions for matrix compressive failure

The fracture angle for pure transverse compression can be considered as $\alpha_o = 53°$ if no experimental value is available. The friction parameter η^T is obtained from

$$\tan(2\alpha_o) = -\frac{1}{\eta^T}, \tag{136}$$

the transverse strength S^T is defined as

$$S^T = Y^C \cos(\alpha_o) \left(\sin(\alpha_o) + \frac{\cos(\alpha_o)}{\tan(2\alpha_o)} \right) \tag{137}$$

and, in the absence of experimental data to obtain η^L, this is defined from the relation

$$\frac{\eta^L}{S^L_{is}} = \frac{\eta^T}{S^T}. \tag{138}$$

The stresses in the potential fracture planes (in the interval $\alpha \in [0, \pi[$) are obtained with

$$\begin{cases} \sigma_n = \dfrac{\sigma_{22} + \sigma_{33}}{2} + \dfrac{\sigma_{22} - \sigma_{33}}{2} \cos(2\alpha) + \tau_{23} \sin(2\alpha) \\ \tau^T = \dfrac{\sigma_{22} + \sigma_{33}}{2} - \dfrac{\sigma_{22} - \sigma_{33}}{2} \sin(2\alpha) + \tau_{23} \cos(2\alpha) \\ \tau^L = \tau_{12} \cos(\alpha) + \tau_{31} \sin(\alpha). \end{cases} \tag{139}$$

Expressions for fiber kinking and for biaxial compressive failure

For the determination of $\gamma^c_{1^m2^m}$, φ^o and φ^c, a two steps solution is required, since kinking can be promoted by instability or matrix failure [5]. The solution for instability results from solving the following system for φ^o and $\gamma^c_{1^m2^m}$

$$\begin{cases} f_{CL}(\gamma^c_{1^m2^m}) = -\dfrac{X^C}{2} \sin\left[2\left(\varphi^o + \gamma^c_{1^m2^m}\right)\right] \\ \left.\dfrac{\partial f_{CL}(\gamma_{1^m2^m})}{\partial \gamma_{1^m2^m}}\right|_{\gamma^c_{1^m2^m}} = -X^C \cos\left[2\left(\varphi^o + \gamma^c_{1^m2^m}\right)\right] \end{cases} \tag{140}$$

and φ^c follows as $\varphi^c = \varphi^o + \gamma^c_{1^m2^m}$. If this solution is verified with $F_M < 1$ (in LaRC04 #2, Eq. (81) or from Table 6), then the instability solution must be considered; otherwise the matrix compressive failure solution is considered, and φ^c, $\gamma^c_{1^m2^m}$ and φ^o are defined as follows:

[5] For a linear material, there is no need to check for the instability solution

$$\varphi^c = \arctan\left(\frac{1-\sqrt{1-4\left(\frac{S^L}{X^C}+\eta^L\right)\frac{S^L}{X^C}}}{2\left(\frac{S^L}{X^C}+\eta^L\right)}\right) \tag{141}$$

$$\gamma^c_{1^m2^m} = f^{-1}_{CL}\left(\frac{1}{2}\sin\left(2\varphi^c\right)X^C\right) \tag{142}$$

where f_{CL} is the in-plane shear constitutive shear law. For a linear behaviour it simplifies to

$$\gamma^c_{1^m2^m} = \frac{\varphi^c X^C}{G_{12}}. \tag{143}$$

Either way, the initial misalignment angle comes then as

$$\varphi^o = \varphi^c - \gamma^c_{1^m2^m}. \tag{144}$$

The plane where kinking takes place is defined by

$$\tan\left(2\psi\right) = \frac{2\tau_{23}}{\sigma_{22}-\sigma_{33}} \tag{145}$$

and the stresses rotated to that plane are

$$\begin{cases} \sigma_{2^\psi 2^\psi} = \dfrac{\sigma_{22}+\sigma_{33}}{2} + \dfrac{\sigma_{22}-\sigma_{33}}{2}\cos\left(2\psi\right) + \tau_{23}\sin\left(2\psi\right) \\ \sigma_{3^\psi 3^\psi} = \sigma_{22}+\sigma_{33}-\sigma_{2^\psi 2^\psi} \\ \tau_{12^\psi} = \tau_{12}\cos\left(\psi\right) + \tau_{31}\sin\left(\psi\right) \\ \tau_{2^\psi 3^\psi} = 0 \\ \tau_{3^\psi 1} = \tau_{31}\cos\left(\psi\right) - \tau_{12}\sin\left(\psi\right). \end{cases} \tag{146}$$

The shear strain in the misalignment frame $\gamma^u_{1^m2^m}$ is obtained by iteratively solving the equation

$$f_{CL}(\gamma_{1^m2^m}) = -\frac{\sigma_{11}-\sigma_{2^\psi 2^\psi}}{2}\sin\left(2\left(\varphi^o+\gamma_{1^m2^m}\right)\right) + \left|\tau_{12^\psi}\right|\cos\left(2\left(\varphi^o+\gamma_{1^m2^m}\right)\right) \tag{147}$$

which, for a linear shear behaviour and with small angle approximation reduces to

$$\gamma_{1^m2^m} = \frac{\varphi^o G_{12}+\left|\tau_{12}\right|}{G_{12}+\sigma_{11}-\sigma_{22}} - \varphi^o \tag{148}$$

and the angle φ comes as

$$\varphi = \frac{\tau_{12^\psi}}{\left|\tau_{12^\psi}\right|}\left(\varphi^o+\gamma_{1^m2^m}\right). \tag{149}$$

Eq. (147) does not always have a solution, since failure by instability is also possible. If, for a specific load state, Eq. (147) does not have a solution (this

can be easily checked by plotting the left and right hand side of the equation in a (γ, τ) space), then failure has taken place by instability. The envelope for failure by instability is defined by the following system:

$$\begin{cases} f_{CL}(\gamma_{1^m2^m}) = -\dfrac{\sigma_{11} - \sigma_{2^\psi 2^\psi}}{2} \sin\left(2\left(\varphi^o + \gamma_{1^m2^m}\right)\right) + \left|\tau_{12^\psi}\right| \cos\left(2\left(\varphi^o + \gamma_{1^m2^m}\right)\right) \\ \dfrac{\partial f_{CL}(\gamma_{1^m2^m})}{\partial \gamma_{1^m2^m}} = -\left(\sigma_{11} - \sigma_{2^\psi 2^\psi}\right) \cos\left(2\left(\varphi^o + \gamma_{1^m2^m}\right)\right) - 2\left|\tau_{12^\psi}\right| \sin\left(2\left(\varphi^o + \gamma_{1^m2^m}\right)\right). \end{cases} \tag{150}$$

If Eq. (147) has a solution (and thus the material has not failed by instability), matrix failure is checked next. After knowing the orientation of the misalignment frame, the stresses can be rotated to it using

$$\begin{cases} \sigma_{1^m1^m} = \dfrac{\sigma_{11} + \sigma_{2^\psi 2^\psi}}{2} + \dfrac{\sigma_{11} - \sigma_{2^\psi 2^\psi}}{2} \cos(2\varphi) + \tau_{12^\psi} \sin(2\varphi) \\ \sigma_{2^m2^m} = \sigma_{11} + \sigma_{2^\psi 2^\psi} - \sigma_{1^m1^m} \\ \tau_{1^m2^m} = -\dfrac{\sigma_{11} - \sigma_{2^\psi 2^\psi}}{2} \sin(2\varphi) + \tau_{12^\psi} \cos(2\varphi) \\ \tau_{2^m3^\psi} = \tau_{2^\psi 3^\psi} \cos(\varphi) - \tau_{3^\psi 1} \sin(\varphi) \\ \tau_{3^\psi 1^m} = \tau_{3^\psi 1^\psi} \cos(\varphi). \end{cases} \tag{151}$$

For biaxial compression failure, the rotation to the potential fracture planes (in the interval $\alpha \in]0, \pi[$) are obtained with

$$\begin{cases} \sigma_n^m = \dfrac{\sigma_{2^m2^m} + \sigma_{3^\psi 3^\psi}}{2} + \dfrac{\sigma_{2^m2^m} - \sigma_{3^\psi 3^\psi}}{2} \cos(2\alpha) + \tau_{2^m3^\psi} \sin(2\alpha) \\ \tau^{Tm} = -\dfrac{\sigma_{2^m2^m} - \sigma_{3^\psi 3^\psi}}{2} \sin(2\alpha) + \tau_{2^m3^\psi} \cos(2\alpha) \\ \tau^{Lm} = \tau_{1^m2^m} \cos(\alpha) + \tau_{3^\psi 1^m} \sin(\alpha). \end{cases} \tag{152}$$

For $\sigma_{2^m2^m} \geq 0$, it is considered that fiber kinking follows matrix failure only if $\sigma_{11} < -X^C/2$.

Appendix - Particularization of the non-linear shear behaviour for a 3^{rd} order polynomial

The LaRC04 criteria presented here accounts for a generic non-linear shear behaviour. Any expression for non-linear shear can be used, such as a polynomial, a logarithmic, any other best fit to experimental data or the experimental data itself. This appendix presents the particularization of the criteria for Hahn and Tsai's 3^{rd} order polynomial representation for shear non-linearity [50]:

$$\gamma_{12} = \frac{1}{G_{12}}\tau_{12} + \beta\left(\tau_{12}\right)^3 \tag{153}$$

with β obtained from the shear tests ($\beta = 0$ for linear behaviour).

Expressions for matrix tensile failure

The in-plane shear strength of thick embedded plies and thin plies have the same general form,

$$S_{is}^{L} = \sqrt{\frac{\left(1 + \beta\phi\left(G_{12}\right)^2\right)^{1/2} - 1}{3\beta G_{12}}} \tag{154}$$

where the parameter ϕ is obtained as:

$$\phi = \frac{12\left(S^L\right)^2}{G_{12}} + \frac{72}{4}\beta\left(S^L\right)^4 \qquad \text{for a thick embedded ply} \tag{155}$$

$$\phi = \frac{48 G_{IIc}}{\pi t} \qquad \text{for a thin ply} \tag{156}$$

A linear shear behaviour is obtained when the constant β tends to zero in Eq. (153)

$$\lim_{\beta\to 0} S_{is}^{L} = \lim_{\beta\to 0}\sqrt{\frac{\left(1 + \beta\phi\left(G_{12}\right)^2\right)^{1/2} - 1}{3\beta G_{12}}} = \sqrt{\frac{\phi G_{12}}{6}}. \tag{157}$$

The particular values of the in-situ shear strengths for a linear shear behaviour can thus be expressed as

$$S_{is}^{L} = \sqrt{2}S^L \qquad \text{for a thick embedded ply} \tag{158}$$

$$S_{is}^{L} = \sqrt{\frac{8 G_{12} G_{IIc}}{\pi t}} \qquad \text{for a thin ply} \tag{159}$$

Initial misalignment angle For the determination of $\gamma^c_{1^m2^m}$, φ^o and φ^c, a two steps solution is required, since kinking can be promoted by instability or matrix failure [6]. The solution for instability results from solving iteratively the following system for φ^o and $\tau^c_{1^m2^m}$

$$\begin{cases} \tau^c_{1^m2^m} = -\dfrac{X^C}{2}\sin\left[2\left(\varphi^o + \frac{1}{G_{12}}\tau^c_{1^m2^m} + \beta\left(\tau^c_{1^m2^m}\right)^3\right)\right] \\ \dfrac{1}{\frac{1}{G_{12}} + 3\alpha\left(\tau^c_{1^m2^m}\right)^2} = -X^C\cos\left[2\left(\varphi^o + \frac{1}{G_{12}}\tau^c_{1^m2^m} + \beta\left(\tau^c_{1^m2^m}\right)^3\right)\right] \end{cases} \tag{160}$$

and then compute $\gamma^c_{1^m2^m}$ and φ^c as

$$\gamma^c_{1^m2^m} = \frac{1}{G_{12}}\tau^c_{1^m2^m} + \beta\left(\tau^c_{1^m2^m}\right)^3 \tag{161}$$

$$\varphi^c = \gamma^c_{1^m2^m} + \varphi^o. \tag{162}$$

If this solution is verified with $F_M < 1$ (in LaRC04 #2, Eq. (81) or from Table 6), then the instability solution must be considered; otherwise the matrix compressive failure solution is considered, and φ^c is determined from Eq. (141), $\gamma^c_{1^m2^m}$ comes from

$$\gamma^c_{1^m2^m} = \frac{1}{G_{12}}\left(\frac{1}{2}\sin\left(2\varphi^c\right)X^C\right) + \beta\left(\frac{1}{2}\sin\left(2\varphi^c\right)X^C\right)^3 \tag{163}$$

and $\varphi^o = \varphi^c - \gamma^c_{1^m2^m}$.

Current misalignment frame The shear strain in the misalignment frame $\gamma_{1^m2^m}$ is obtained by iteratively solving the equation

$$\gamma_{1^m2^m} = \frac{1}{G_{12}}\tau^*(\gamma_{1^m2^m}) + \beta\left[\tau^*(\gamma_{1^m2^m})\right]^3 \tag{164}$$

with

$$\tau^*(\gamma_{1^m2^m}) = -\frac{\sigma_1 - \sigma_{2^\psi}}{2}\sin\left(2\left(\varphi^o + \gamma_{1^m2^m}\right)\right) + \left|\tau_{12^\psi}\right|\cos\left(2\left(\varphi^o + \gamma_{1^m2^m}\right)\right). \tag{165}$$

Eq. (164) does not always have a solution, since failure by instability is also possible. If, for a specific load state, Eq. (164) does not have a solution (this can be easily checked by plotting the left and right hand side of the equation), then

[6] For a linear material, there is no need to check for the instability solution

failure has taken place by instability. The envelope for failure by instability is defined by the following system:

$$\begin{cases} \tau_{1^m 2^m} = -\dfrac{\sigma_{11}-\sigma_{2^\psi 2^\psi}}{2}\sin\left(2\left(\varphi^o+\frac{1}{G_{12}}\tau_{1^m 2^m}+\beta\left(\tau_{1^m 2^m}\right)^3\right)\right)+ \\ +\left|\tau_{12^\psi}\right|\cos\left(2\left(\varphi^o+\frac{1}{G_{12}}\tau_{1^m 2^m}+\alpha\left(\tau_{1^m 2^m}\right)^3\right)\right) \\ \dfrac{1}{\frac{1}{G_{12}}+3\beta\left(\tau_{1^m 2^m}\right)^2} = -\left(\sigma_{11}-\sigma_{2^\psi 2^\psi}\right)\cos\left(2\left(\varphi^o+\frac{1}{G_{12}}\tau_{1^m 2^m}+\beta\left(\tau_{1^m 2^m}\right)^3\right)\right)- \\ -2\left|\tau_{12^\psi}\right|\sin\left(2\left(\varphi^o+\frac{1}{G_{12}}\tau_{1^m 2^m}+\beta\left(\tau_{1^m 2^m}\right)^3\right)\right). \end{cases} \tag{166}$$

REPORT DOCUMENTATION PAGE

Form Approved
OMB No. 0704-0188

1. REPORT DATE *(DD-MM-YYYY)*	2. REPORT TYPE	3. DATES COVERED *(From - To)*
01- 02 - 2005	Technical Memorandum	

4. TITLE AND SUBTITLE

Failure Models and Criteria for FRP Under In-Plane or Three-Dimensional Stress States Including Shear Non-Linearity

5a. CONTRACT NUMBER

5b. GRANT NUMBER

5c. PROGRAM ELEMENT NUMBER

6. AUTHOR(S)

Pinho, Silvestre T.; Davila, Carlos G.; Camanho, Pedro P.; Iannucci, Lorenzo; and Robinson, Paul

5d. PROJECT NUMBER

5e. TASK NUMBER

5f. WORK UNIT NUMBER

23-064-30-22

7. PERFORMING ORGANIZATION NAME(S) AND ADDRESS(ES)

NASA Langley Research Center
Hampton, VA 23681-2199

8. PERFORMING ORGANIZATION REPORT NUMBER

L-19089

9. SPONSORING/MONITORING AGENCY NAME(S) AND ADDRESS(ES)

National Aeronautics and Space Administration
Washington, DC 20546-0001

10. SPONSOR/MONITOR'S ACRONYM(S)

NASA

11. SPONSOR/MONITOR'S REPORT NUMBER(S)

NASA/TM-2005-213530

12. DISTRIBUTION/AVAILABILITY STATEMENT

Unclassified - Unlimited
Subject Category 39
Availability: NASA CASI (301) 621-0390

13. SUPPLEMENTARY NOTES

Pinho, Iannucci, and Robinson: Imperial College; Davila: Langley Research Center; Camanho: University of Porto
An electronic version can be found at http://ntrs.nasa.gov

14. ABSTRACT

A set of three-dimensional failure criteria for laminated fiber-reinforced composites, denoted LaRC04, is proposed. The criteria are based on physical models for each failure mode and take into consideration non-linear matrix shear behaviour. The model for matrix compressive failure is based on the Mohr-Coulomb criterion and it predicts the fracture angle. Fiber kinking is triggered by an initial fiber misalignment angle and by the rotation of the fibers during compressive loading. The plane of fiber kinking is predicted by the model. LaRC04 consists of 6 expressions that can be used directly for design purposes. Several applications involving a broad range of load combinations are presented and compared to experimental data and other existing criteria. Predictions using LaRC04 correlate well with the experimental data, arguably better than most existing criteria. The good correlation seems to be attributable to the physical soundness of the underlying failure models.

15. SUBJECT TERMS

Failure criteria; Matrix cracks; Fiber kinking; Damage; Composite materials

16. SECURITY CLASSIFICATION OF:			17. LIMITATION OF ABSTRACT	18. NUMBER OF PAGES	19a. NAME OF RESPONSIBLE PERSON
a. REPORT	b. ABSTRACT	c. THIS PAGE			STI Help Desk (email: help@sti.nasa.gov)
					19b. TELEPHONE NUMBER *(Include area code)*
U	U	U	UU	69	(301) 621-0390